C 4 Complex Magnetism[1]

Stefan Blügel
Peter Grünberg Institut
and
Institute for Advanced Simulation
Forschungszentrum Jülich GmbH

Contents

1 Introduction to Complex Magnetism

Probably the most known manifestation of magnetism is ferromagnetism. Ferromagnetic materials are important constituents of many modern hi-tech devices. For example, more than 90% of all information world-wide is stored in ferromagnetic domains. Ferromagnetism is a form of magnetism, characterized at equilibrium by an additional macro-variable, the *spontaneous magnetization* $\boldsymbol{M}$, – a temporally stable *spontaneous collective ordering* of permanent magnetic moments typically of magnetic atoms – of a solid at temperatures below a critical temperature $T_{\rm c}$, called Curie temperature, $T_{\rm C}$, $T_{\rm C} = T_{\rm c}$, in case of ferromagnets. Above the critical temperature the spontaneous magnetization remains zero and the solid behaves like normal paramagnets. The disappearance of the spontaneous magnetization is an example for a phase transition of second order where the spontaneous magnetization is the order parameter characterizing the phase transition, vanishing continuously at $T_{\rm c}$. For second order phase transitions an important principal exists, namely *universality*. Universality means that the behavior of a system close to its critical point does not depend on details of the system such as its material parameters or the geometry of the sample. Instead, physical systems fall into so-called *universality classes* depending only on symmetry of the underlying model such as the spatial dimension of the system, or – in a magnetic system – the dimension of the spins. On the other hand the Curie temperature is a material dependent quantity, and a very important one. Since for technological applications magnetic devices must have operating temperatures of about room temperature or even higher, the understanding of the influence of the critical temperature on the detailed properties of the magnetic systems is an important part of today's research. This is discussed in much more detail in the lecture C1 of Phivos Mavropoulos.

For many magnets the permanent magnetic moments still exist above $T_{\rm c}$, but the magnetic moments are disordered. It may seem at first paradoxically that a disordered high-temperature phase is more symmetric than the low-temperature ordered state, but this is a quite general phenomenon. For example, a uniform liquid state (e.g. water) is invariant under arbitrary translations in space, while a crystal (e.g. ice) is only invariant under translations by an integer number of lattice constants. In fact, in most phase transitions some symmetry of the high-temperature phase becomes broken when an ordered state sets in. For example, ferromagnetic ordering breaks time reversal symmetry, i.e. if $T : t \longrightarrow -t$ then $\mathrm{M} \longrightarrow -\mathrm{M}$, because the magnetization M (average magnetic moment per unit volume) appearing below the transition temperature changes sign under time reversal. Such a symmetry breaking is called spontaneous, which means the Hamiltonian describing the system is invariant under a symmetry transformation, while the ordered state is not. See for example the Heisenberg exchange interaction, discussed in Section 2.1, which is invariant under time reversal symmetry since both $\mathbf{S}_i$ and $\mathbf{S}_j$ change sign when $t \longrightarrow -t$, while an ordered spin state with a nonzero average spin $\langle \mathbf{S} \rangle$ is not.

Magnetism is the science of cooperative effects of orbital and spin moments in matter, and ferromagnetism is one example of it. Actually all condensed matter shows a magnetic response to the presence of an applied magnetic field. The magnetizibility or susceptibility can vary greatly in both strength, by over 10 orders of magnitude, and manner. Some solids exhibit even a magneto-electric response, i.e. a magnetic response when an electric field is a applied. The response is used to classify solids for example in diamagnets, paramagnets or ferromagnets. Magnetism is a *quantum many-body phenomenon.* All-in-all, already in 1926, independent of each other, Dirac and Heisenberg recognized the quantum mechanical exchange interaction in competition to the kinetic energy of the moving electrons as the decisive origin of collective magnetism. The exchange interaction is a result of the electrostatic Coulomb interaction

between the electrons in concert with the antisymmetric nature of the many–electron wavefunction (Pauli principle). The strength of the exchange interaction is much modified by the electron correlation of the interacting electrons. More precisely, magnetism is a relativistic quantum phenomenon and their is probably no field of condensed matter where the spin-orbit interaction has so many different ramifications. Well-known and practically important manifestations of spin-orbit effects in magnets and spin-transport are the magnetic anisotropy, the anisotropic exchange, the antisymmetric exchange often referred to as Dzyaloshinskii-Moriya interaction, the tunnelling anisotropic magnetoresistance (TAMR), the anomalous and the spin-Hall effect, as well as their quantum counterparts, of the Elliot-Yafet, D'yakonov-Perel and Bir-Aronov-Pikus spin-relaxation mechanisms in electron transport, etc. For more details see also the lectures A6, A10, C6 of Yuriy Mokrousov, Gustav Bihlmayer, and Samir Lounis, respectively.

The quantum states of electrons vary tremendously from solid to solid if we consider that we deal with insulators, semiconductors, metals, oxides, molecular materials, crystalline, amorphous and glassy solids, liquids, heterostructures, thin films, quasi-one dimensional chains, clusters, single molecules giving rise to a rich spectrum of *exchange interactions* (for simplicity one refers frequently simply to: interactions between magnetic moments) connecting over distances the little permanent magnetic moments constituting the solid. We may deal with long- and short-ranged interactions, interactions that produce ferromagnetic or antiferromagnetic alignment of spins between different pairs of atoms, whose strength and alignment type may depend on the distance. This leads to a large variety of magnetic behaviors such as spin glass, spin liquids or spin ice and very different magnetic phases, e.g. *collinear magnetic phases* as for the ferromagnetic (FM), antiferromagnetic (AFM), ferrimagnetic (FIM), and sinusoidal spin-density wave phase (sSDW), or *non-collinear chiral and achiral magnetic phases* as for planar and conical helicoidal (HSDW) and cycloidal spin-density wave phase (CSDW) characterised by a single or multiple wave vector $\mathbf{q}$ states. (Please notice sSDW or SDW denotes the sinusoidal spin-density wave, while SSDW denotes the spiral spin-density wave, such as the HSDW and the CSDW.)

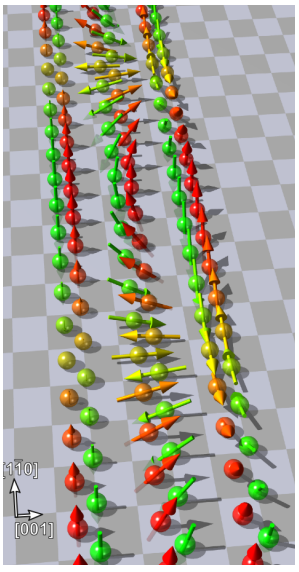

Fig. 1: *From left to right illustration of a single-q sinusoidal, helical and cycloidal spin-density wave of an AFM double chain (from [1]).*

Usually the full fermionic degree of freedom of the electronic quantum many-body problem is too large to discuss all these experimental observations effectively. Therefore, effective spin-models (see Section 2) have been developed that catch or try to catch the major microscopic exchange mechanism and reduce the problem to the spin-degree of freedom, by which the electron degree of freedom and the electronic structure is summarised by exchange parameters. One of the most familiar spin-models is the Heisenberg model (see Section 2.1) with the exchange interaction $J_{i,j}$ between atoms at sites i, and j. The presence of the spin-Hamiltonian bears various advantages, it permits (i) an efficient search for the magnetic ground-state, (ii) the calculations of dynamical properties such as the magnon dispersion or magnetic excitations and (iii) the calculation of thermal properties such as the critical temperature. In the last years there is an effort to calculate the exchange parameter from first-principles and enable the development of *realistic model Hamiltonians*, thus being able to model realistic systems.

In the past decade we witnessed a multitude of investigations of non-collinear magnetism in the context of first-principles theory, where solutions of both the spiral spin-density wave and

complex non-collinear magnetic structures have been found, first for simple, but now also for more complicated systems. Interesting steps are undertaken to explore the potential ground state magnetic structure, investigate the spin-dynamics or describe the thermodynamics properties in magnets. After the thorough discussion of density functional theory for a non-collinear magnet was completed in Ref. [2], the successful calculations established the density functional theory as a powerful tool to investigate these complex magnets, in particular complex itinerant magnets. For a deeper and broader introduction to the field, following books and general reviews are recommended: [3, 4, 5, 6, 7].
In this Lecture, at first a brief introduction to the field of complex magnetism is given , and then an extension of the spin-density functional theory to non-collinear magnetism is introduced. Then, different strategies are provided in how to use the description of the non-collinear magnetism to find ground-states in complex magnets and the use of the adiabatic principle to calculated magnon and thermal properties. A slight emphasis is given to chiral magnetism, a field that enjoys currently considerable attention. Finally, some examples are discussed, taken from the field of magnetism in reduced dimension, i.e. thin films and clusters at surfaces, at which a lot of interesting new physics was observed recently.

1.1 Collinear magnetism

In collinear magnets there is a common magnetization axis $\hat{\mathbf{e}}_M$ for all atoms, for which for convenience the z-axis is chosen. In ferromagnets ($\uparrow\uparrow\uparrow\cdots$) the magnetic moment $M_i = M$ has the same value at all sites i, with the position of the atomic nucleus denoted by $\mathbf{R}_i$. An (Nèel) antiferromagnet ($\uparrow\downarrow\uparrow\cdots$) has a staggered arrangement of magnetic moments $M_i = \pm M$ of the same size, but opposite sign at neighboring sites. In real solids one can find, however, also more complicated forms of antiferromagnetism, e.g. the so-called "up-up-down-down" state ($\uparrow\uparrow\downarrow\downarrow\uparrow\cdots$). In ferrimagnets ($\uparrow\downarrow\uparrow\cdots$) magnetic moments $M_{\tau,i} = M_\tau$ of all sites i at each sub-lattice τ are the same, but different to a different sub-lattice τ', $M_\tau \neq M_{\tau'}$.
Best known representatives of ferromagnets and antiferromagnets are the elemental $3d$ transition-metals (see also Fig. 2): bcc-Fe, hcp-Co and fcc-Ni are ferromagnetic in the elemental ground state lattice, bcc-Cr and fcc-Mn (high-temperture phase of Mn) are antiferromagnetic. Actually the magnetism of Cr and Mn is much more complicated. Cr shows a frozen sinusoidal spin-density-wave behavior, whose magnetism is characterized by a magnetization, which varies in space like a wave, and which integrated over space, leads to a vanishing total magnetization:

$$\mathbf{m}(\mathbf{r}) = \mathbf{M}\cos\mathbf{q}\mathbf{r} \qquad \int_\infty \mathbf{m}(\mathbf{r})d\mathbf{r} = 0\,. \tag{1}$$

For the ground state of Cr the experimental result $q \approx 0.952\frac{2\pi}{a}$ represents an *incommensurate* spin-density wave as sketched in Fig. 2. The magnetic and structural periodicities are *incommensurately* different. The antiferromagnetism of Cr and its spin-density-wave behavior have recently received considerable new attention, both experimentally [8] and theoretically [9]. In my opinion the frozen sSDW of Cr could not be explained satisfactorily yet on a quantitative level by density functional theory. Obviously, the ferromagnetic state with $\mathbf{q} = (0,0,0)$, and the Nèel antiferromagnetic state are particular examples of the frozen sSDW state. For the "antiferromagnetic approximation" of bcc Cr and γ-Mn, the high-temperature fcc phase of Mn, the wave vector of the magnetization points along one of the cubic axes: $\mathbf{q} = (0,0,q)$ with $q = 2\pi/a$ and positive and negative magnetization are alternating in z direction. Actually "an-

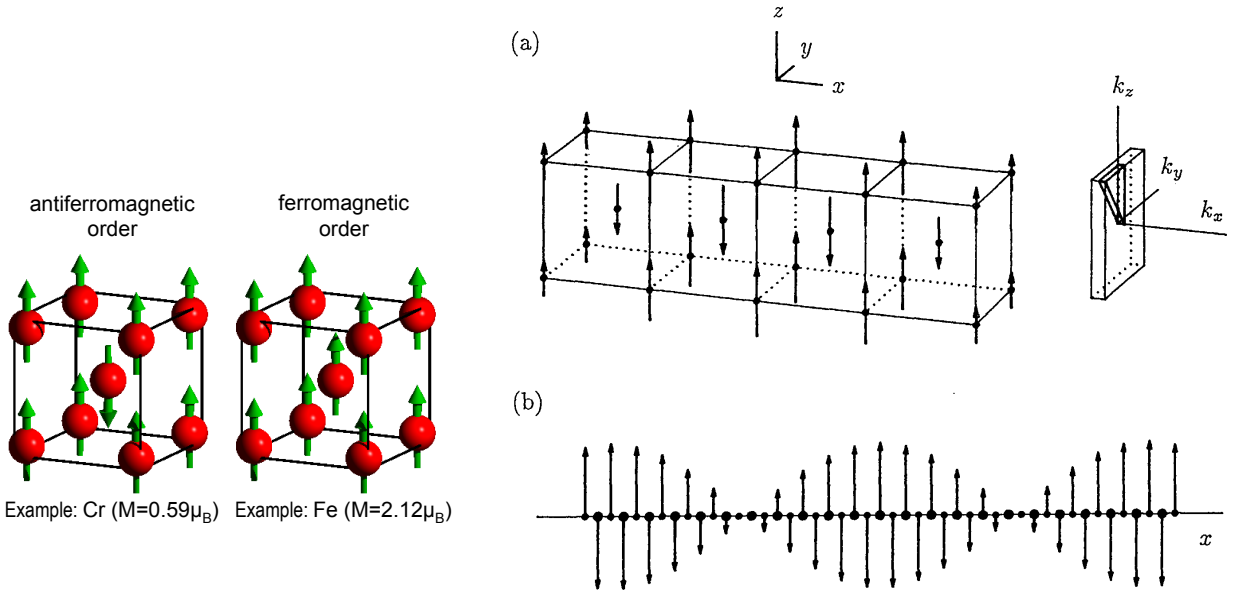

Fig. 2: *Left panel, antiferromagnetic and ferromagnetic structure of bcc Cr and Fe. Right panel, sinusoidal spin density wave in a bcc lattice after Hirai [10]: (a) for* $q = \frac{11}{12}\frac{2\pi}{a}$ *in the region of maximal moments, (b) for* $q = 0.952\frac{2\pi}{a}$*, where the arrows mark the direction and the size of the moments. Small points mark corner atoms, large points central atoms in the bcc unit cell.*

tiferromagnetic" Mn at room temperature has a complicated unit cell containing 58 atoms and will not be considered here any further.
Another well-known example of collinear magnets comes from the field of transition-metal oxides. Transition-metal oxides can be magnetic and they can exhibit a very rich spectrum of magnetic phases. Historic examples include the perovskite compounds $(La_{1-x}Ca_x)MnO_3$ [11]. As function of the Ca concentration x this series of compounds exhibits ferromagnetic (FM) and antiferromagnetic (AFM) properties, which depend upon the relative trivalent and tetravalent manganese ion content. The samples are purely ferromagnetic over a relatively narrow range of composition ($x \sim 0.35$) and show simultaneous occurrence of ferromagnetic and antiferromagnetic phases in the ranges ($0 < x < 0.25$) and ($0.40 < x < 0.5$). Several types of antiferromagnetic structures at $x = 0$ and $x > 0.5$ have been determined. According to the work of Wollan and Koehler [11] one classifies the type of antiferromagnetic phase as AFM-A to AFM-G phase. Fig. 3 gives some examples.
Metallic ferrimagnets are found in compounds containing $4f$ and $3d$ elements. Examples, are the Laves phase compounds, e.g. $GdFe_2$, $Gd_{1-x}Y_xFe_2$, $CeFe_2$. A well-known class of examples of insulating ferrimagnets are the ferrites, e.g. $FeO.Fe_2O_3$, $NiO.Fe_2O_3$, $CuO.Fe_2O_3$, ... in the spinel structure. They contain different transition-metal ions (or in case of magnetite Fe_3O_4, it contains two inequivalent iron atoms with two different valencies) carrying two different magnetic moments.

1.2 Non-collinear magnetism

In noncollinear magnetic structures, the magnetization axis $\hat{\mathbf{e}}_M^i$ is not the same for all atoms and in fact it can change direction from site to site. Noncollinear magnetic structures were first

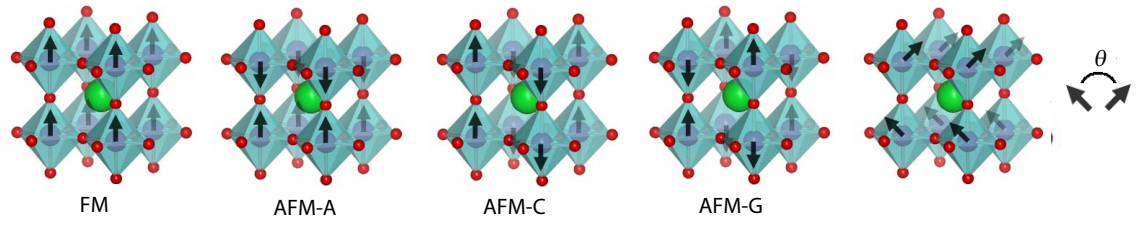

Fig. 3: *Examples of collinear ferromagnetic (FM) and antiferromagnetic (AFM) magnetic states as typical for perovskites, e.g. $(La_{1-x}Sr_x)MnO_3$ (La or Sr, biggest ball green; Mn, mid-size ball blue; O, tiny ball red): FM, AFM-A, AFM-C and AFM-G states, respectively, following the Wollan-Koehler notation [11]. The outer right image represents a non-collinear magnetic state, with a quantization axis, whose direction changes from plane to plane by an angle θ.*

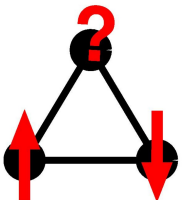

Fig. 4: *Illustration of frustration of AFM interaction between pairs of atoms on triangular lattice.*

discovered experimentally [12, 13] about 50 years ago. Non-collinear magnetism in general and incommensurate spiral spin-density waves in particular are complex magnetic structures which exist in a variety of systems. They often occur in systems with a (i) topologically frustrated antiferromagnetic interaction, e.g. such as for antiferromagnetically interaction magnetic atoms on a triangular lattice, disordered systems, spin-glasses, or (ii) in materials with competing exchange interactions between different neighbors as for example for fcc Fe, the helimagnetism of the lanthanides (see Fig. 5), and multi-component magnets, e.g. $LaMn_2Ge_2$ (see Fig. 12), in exchange bias systems, and molecular magnets, or (iii) on a longer scale in materials with competing interactions of different type, e.g. domain wall. In (i) and (ii) the complex magnetic structure comes purely from exchange and therefore the spiral-states in those helimagnets are often called exchange spirals.

To give the reader at least an example of the richness of the possible magnetic phases I present a series of insulating rare earth (R) perovskites $R\mathrm{MnO_3}$ (R =La, Pr, Nd, ...). $R\mathrm{MnO_3}$ systems crystallize in a perovskite structure with a large $\mathrm{GdFeO_3}$-type distortion [14]. With changing the rare earth atom from La with a large ionic radius to the small ionic radius of Er, the bond angles of Mn-O-Mn decrease and the $\mathrm{GdFeO_3}$-type distortions increase. It was reported on ground of experiments [15], that the magnetic ground state changes from A-type antiferromagnetic (AFM-A) (Fig. 6(a)) to incommensurate magnetic (spiral) state (Fig. 6(d)) to E-type antiferromagnetic (AFM-E) (Fig. 6(c)). The spin-ordering temperatures of $R\mathrm{MnO_3}$ as a function of the in-plane Mn-O-Mn bond angle is shown in Fig. 6.

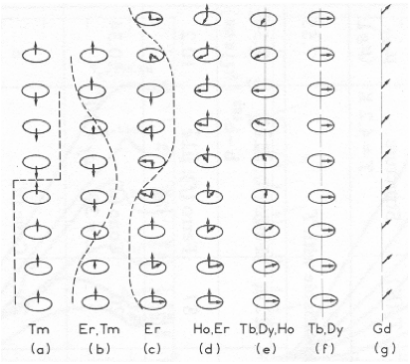

Fig. 5: *Helimagnetism of some $4f$-metals.*

The helimagnetic state of the lanthanides looks like a snapshot of a single magnon at a fixed time. Therefore, these ground states are often called frozen magnons. A magnon is a collective excitation, where the local magnetic moments deviate slightly from the ferromagnetic ground state (or any other magnetic state as ground state) and are typically not stationary states.

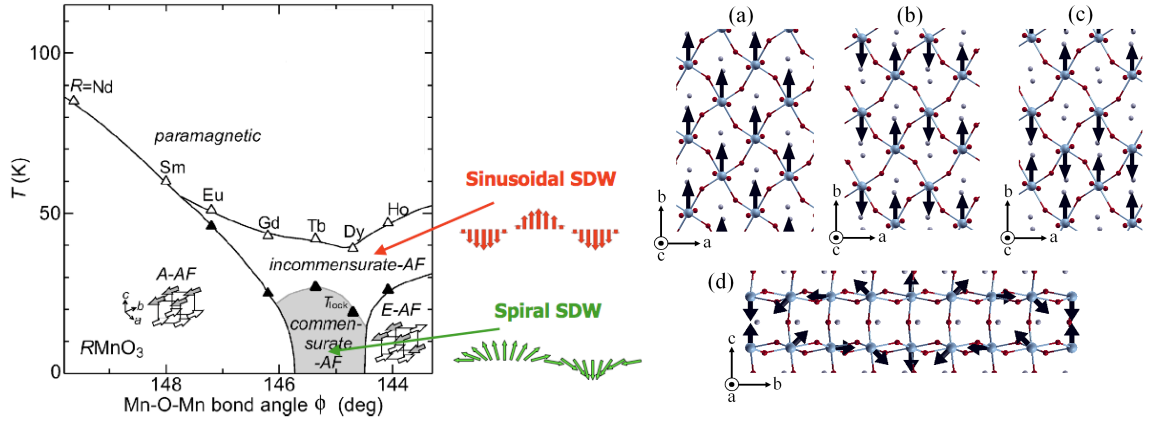

Fig. 6: *Left figure: Spin-ordering temperatures of rare earth (R =Nd, ..., Ho) $RMnO_3$ as a function of the in-plane Mn-O-Mn bond angle according to Kimura et al. [15]. Right figure: Magnetic structures of $RMnO_3$. Black arrows and large gray spheres denote the spin and Mn atoms, respectively. Small gray and red spheres denote the rare earth (R) and O atoms, respectively. All magnetic structures in this figure exhibit an AFM coupling along the c-axis. (a), (b) and (c) are AFM-A, AFM-G and AFM-E, respectively. (d) describes the spiral magnetic structure with a rotation angle of 45° from site to site along the spin-spiral propagation direction.*

In order to relate the frozen magnon state with the dynamical magnon one relies on an *adiabatic hypothesis*, which conjectures that the slow motion of low-energy magnetic excitations can be decoupled from the fast motion of intersite electron hopping, so that the local electronic structure has time to relax under the constraint that a magnon traverses the system. Under this assumption, the spin-spiral state can therefore be used to simulate the magnon dispersion of a magnetic system in the adiabatic approximation, in particular at very low temperatures, when magnons with long wavelength dominate. At higher temperatures, directional fluctuations of local moments reduce the magnetization. In one-component systems it is well known that the magnetic configuration at each instant shows some degree of short-range order: small regions present almost collinear magnetic moments, with a local spin-quantization axis $\hat{\mathbf{e}}_{\mathrm{eloc}}$ not necessarily parallel to the average moment (the global axis $\hat{\mathbf{e}}_{\mathrm{glob}}$). Thus, under the adiabatic assumption, a non-collinear turn magnetic state can be understood as a snapshot of such a thermal fluctuation. This in shows the potential that arises if one is able to study the non-collinear state one a sophisticated level by a materials dependent theory, such as the spin-dependent density functional theory.

1.3 Exchange mechanisms

In insulating materials the exchange interaction $J_{i,j}$ is typically short-ranged. There exist two categories of types of magnetic interaction:
(i) Direct (potential) exchange: This is driven by minimising potential energy, by reducing wavefunction overlap. Wavefunction overlap is reduced by adding nodes to the wavefunction. This can be done by producing antisymmetric spatial wavefunctions, and so favors symmetric spins, i.e. *ferromagnetic* interactions. This case arises when electrons occupy wavefunctions that overlap in space. In case of wavefunctions localized on different ions the minimization

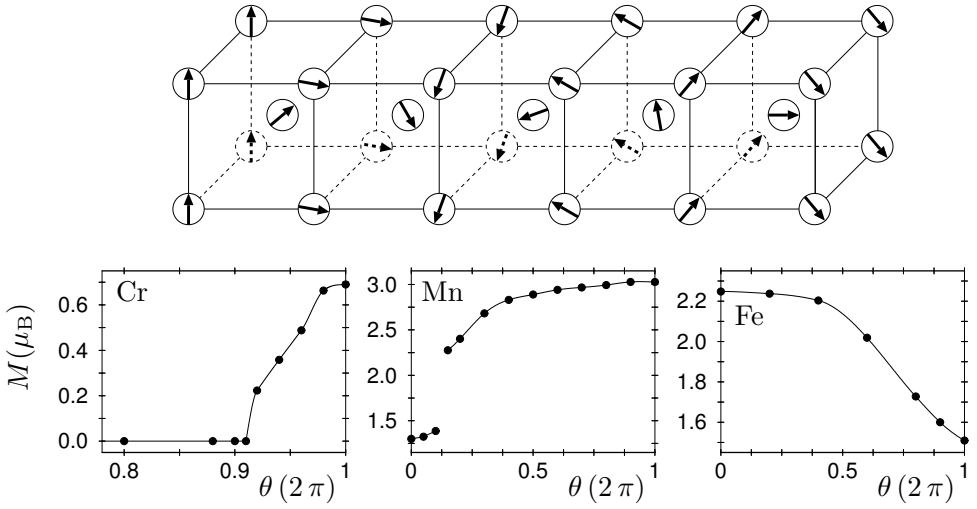

Fig. 7: *Change of the local magnetic moments M in bcc Cr, Mn, and Fe metals as function of the angle θ between the magnetization axes of two consecutive (001) planes. Magnetic moments are aligned ferromagnetically within each (001) plane. Results are calculated for the experimental lattice constants. ($\theta = 2\pi$) $\theta = 0$ corresponds to the (anti-)ferromagnetic state.*

of the Coulomb energy between the different ions lead to symmetric spatial wavefunctions favoring antisymmetric spins, i.e. *antiferromagnetic* interactions.

(ii) Kinetic exchange: This is driven by minimising kinetic energy, by reducing gradients of wavefunctions, i.e. allowing delocalisation of electrons. In insulating compounds with localized electrons the dominating kinetic exchange interaction arises from a process in perturbation calculation involving virtual electron transfer; the resulting interaction is usually *antiferromagnetic*. Kinetic exchange is also sometimes referred to as *superexchange*; we will not use this terminology, as we will use superexchange to refer to a generalisation of this idea, involving hopping via intermediate atoms. This is the historic use of terminology: In this case that transition-metal atoms are that *super* far apart that there is no direct overlap, but still have a strong kinetic exchange. There is an other mechanism favoring ferromagnetism that we can trace back to the discussion of the *double exchange* interaction proposed by Zener [16] for mixed valence manganates in which we have an real exchange of electrons. *Zener's s-d exchange* [17] is a particular mechanism on the basis of kinetic exchange.

There is a potential confusion in the above: these two effects compete, and it is not immediately clear whether in a given situation it is more important to delocalise electrons, or prevent their overlap with other electrons.

(iii) Metallic exchange: In magnetic insulators, the electrons are properly associated with particular atomic sites and the magnetism depends mostly on local or intra–atomic quantities. In metallic materials the exchange interaction is typically long-ranged due to the presence of a Fermi-surface. Magnetism is typically introduced by the $3d$ transition-metal or lanthanide atoms. For example, in $4f$-systems, the exchange interaction between $4f$ localized moments is mediated by $5d$ and $6s$ itinerant electrons and takes the form of a Ruderman-Kittel-Kasuya-Yoshida-type (RKKY) interaction $J(R_j) \propto \cos 2k_F R_j / R_j^3$, for $R_j \ll 1/k_F$, with k_F being the Fermi wave vector, and R_j is the distance of atom j with respect to atom i.

For *itinerant magnetism* or metallic magnetism typical for $3d$-metals, respectively, the electrons responsible for the existence of magnetism hop across the lattice, and thus probe the lattice

and take part in the formation of the Fermi surface. Thus magnetism is intimately interwoven with the electronic structure of the systems. Likewise, the electronic structure is dependent on the atomic arrangement, the composition, and the dimensionality of the system. In transition metals the hopping electrons are correlated, i.e. electrons which hop in and out at a given atomic site share the same orientation of the magnetic spin moment. This finally leads to stable, quasi static local magnetic moments at a given site when averaged over times long compare to hopping times, which are in the order of femto-seconds. This is different to Na, for example, which has fluctuating magnetic moments on the femto-second time scale due to hopping electrons, but no local moment after time averaging. In the spirit of an adiabatic approximation [18, 19] these local magnetic moments may then be treated as classical degrees of freedom relevant to describe pico-second spin dynamics and statistical physics. A typical character of itinerant magnetism is that the magnetic moments are in general not integer, but real numbers, and the value of the moment depends on their relative orientation. This is quantitatively shown in Fig. 7 for bcc Cr, Mn, and Fe.

1.4 Chiral magnetism

Chiral magnets are a particular type of non-collinear magnets that deserve a special mentioning. Systems with lattices lacking inversion symmetry, develop in addition to the above exchange interaction a spin-orbit caused Dzyaloshinskii-Moriya-type [20, 21] antisymmetric exchange interaction, which is one source of origin for multiferroicity in complex oxides and is the origin of the weak ferromagnetism of Fe_2O_3, or of the actinide compounds U_3X_4 (X = P, As or Sb) and U_2Pd_2Sn, to name, but a few popular cases.

Consider a magnetic dimer of two identical magnetic atoms (e.g. blue atoms in Fig. 8) with magnetic moments of unit length, $\mathbf{m} = \hat{\mathbf{e}}$, that are ferromagnetically (↑↑) aligned. If we consider the energy change upon rotating one of the spins, then the energy increase is symmetric with respect of the rotation direction of the moment, say clockwise (↑→), $\mathbf{c} = \hat{\mathbf{e}}_y$, or counterclockwise (↑←), $\mathbf{c} = -\hat{\mathbf{e}}_y$, measured in terms of the vector chirality, $\mathbf{c} = \mathbf{m}_i \times \mathbf{m}_j$, between the magnetic moment $\mathbf{m}_i$ and $\mathbf{m}_j$, if the exchange interaction is caused by the Coulomb interaction. But this is different for the Dzyaloshinskii-Moriya-type (DM) of interaction, which is a chiral interaction, in which one of the two directions is preferred. Thus, the DM-type interaction tries to destabilise a collinear magnetic state (→←) and can introduce a canting of two magnetic moments at different sites (↘↙) or (↗↖), with one of which having a lower energy than that original collinear antiferromagnetic state (→←). Consistent with the periodic lattice of the crystal the ground state for most of the known chiral magnets corresponds to a spiral state. The periodicity of the spiral is given by an interplay between the DM interaction and the Heisenberg exchange. Of course as said in Section 1.2, spiral states may also be supported in non-chiral magnets. In that case, they can result from competing Heisenberg exchange interactions between different neighbors or are due to geometrical frustration and thus are termed exchange spirals. The main feature, which distin-

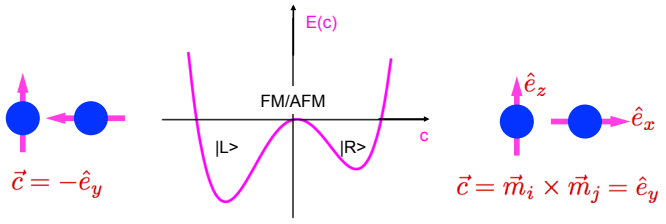

Fig. 8: *Schematic representation of energy versus chirality for a magnetic dimer, represented by two big blue dots. Counterclockwise magnetic structure* $|\mathsf{L}\rangle$ *has lower energy than clockwise rotating structure* $|\mathsf{R}\rangle$.

guishes chiral spirals from exchange ones, is their unique sense of rotation of the magnetization also known as *chirality*.

Chirality is an important property of such magnets. In particular, it supports the stabilization of so-called topologically protected localized magnetic states. Such topologically protected states may occur in chiral magnets as stable or metastable solutions and can be thought of as a two-dimensional analog of the well-known soliton solutions. For the first time, Bogdanov *et al.* [22, 23] has found such solutions in micromagnetic models describing bulk helimagnets, solutions that are now known as chiral magnetic skyrmions. Skyrmions are solutions of smooth non-linear fields [24]. Their topological properties are expressed by a topological number Q, also called winding or skyrmion number, that measures the winding of the magnetic structure when mapped to a unit sphere. For skyrmions, this winding number is a non-zero integer, that means it is not possible to unwind the magnetic structure by external magnetic fields of reasonable strength into a topologically different magnetic structure, e.g. a ferromagnetic state is characterized by a skyrmion number $Q = 0$. Unwinding a skyrmion into a magnetic state with a different topological number goes along with a discontinuous rupture of the smooth skyrmion, which is accompanied by large energy barriers, which effectively makes skyrmions to topologically protected magnetic configurations. Unlike magnetic vortices in nano-discs and magnetic bubbles [25], skyrmions in chiral magnets are stabilized by intrinsic forces, which means that the stabilization of skyrmions does not require particular boundary conditions. Because of the topological protection and localization of the solutions, skyrmions exhibit particle-like properties making them attractive for fundamental research as well as for future applications in various fields, e.g. in *spintronics* [26]. Along this line, a non-zero winding number of a magnetic structure bears some direct physical manifestations in terms of emergent electrical and magnetic fields [27], and electron transport phenomena such as the topological Hall effect [28, 29].

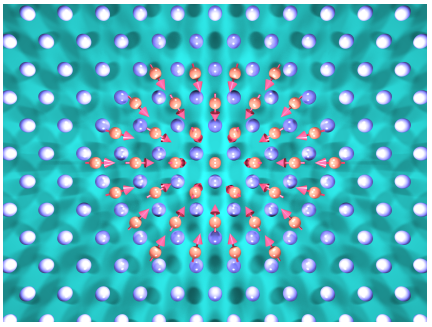

Fig. 9: *Skyrmion with magnetic moments (red arrows) exhibiting a clockwise cycloidal rotation locked in a monatomic cluster (red atom with arrows) deposited on a surface (blue-white atoms).*

Interest in chiral magnets surged after recent experiments confirmed the existence of skyrmions in helimagnets using complementary experimental techniques, neutron scattering [30] and Lorentz microscopy [31]. The bulk and thick-film chiral magnets that are currently under intensive scrutiny are the bulk inversion-asymmetric (BIA) cubic helimagnets, e.g. MnSi [30, 32], $Fe_xCo_{1-x}Si$ [31], MnGe [33], FeGe [34, 35], $Mn_{1-x}Fe_xGe$ [36, 37]. There is a track record of experience and knowledge of these materials that goes back to the investigation to the bulk helimagnets studied in the 70's [38].

1.5 Magnetism in low dimensions

Films and nano-clusters on surfaces constitute a rather new field of complex magnetism. (111) oriented substrates provide triangular lattices on which the materials with antiferromagnetic nearest neighbor interaction is frustrated. In low-dimensional systems the coordination number of neighboring atoms is reduced and the balance between on-site Coulomb interaction and kinetic energy of the moving electron is changed towards the on-site exchange strength, which increases in almost all metal films the magnetic moments. Larger magnetic moments support

higher order exchange interactions that lead to much more complex magnetic structures (see for Example 6.2). Then, magnetic films or clusters on surfaces, or sandwiched multilayers or heterostructures experience the presence of an interface. This interface breaks the structure inversion symmetry (SIA) that gives rise to the antisymmetric exchange interaction, whose strength is among other factors determined by the strength of the spin-orbit interaction of the constituent materials.
In this context, recently, a completely new class of chiral magnets has been established, which are made of monolayers and ultrathin films of transition metals (TM), where the DM interaction and the magnetic chirality is introduced exactly by SIA due to the presence of surfaces and interfaces. In some instances the DM interaction introduces chiral ground states, e.g. in Mn/W(110) [1], Mn/W(100) [39], Fe/Ir(111) [40, 41, 42], Pd/Fe/Ir(111) [43], bi-atomic Fe chains on the (5×1)-Ir(001) surface [44] in other instances chiral domain walls, e.g. in Fe/W(110) [45, 46], Ni/Fe/Cu(001) [47] or the chirality alters dynamical properties as for the magnon dispersion in Fe/W(110) [48].

2 Spin Models

2.1 Heisenberg model

Assuming strong (size is independent of relative orientation to other moments) local magnetic moment formation e.g. at $3d$ transition-metal sites through intraatomic exchange (Hund's 1^{st} rule), we can now attempt to predict how the local spins cooperate on a global length scale at finite temperature, to explain the magnetic ground state of magnetic transition-metal systems or how they respond to excitations. This, however, can be a highly nontrivial task. In cases, for example, where competing exchange interactions between neighboring transition-metal atoms cannot be satisfied, exchange interactions are frustrated giving rise to a multitude of possible spin-structures depending on slight modifications of the exchange interactions. A trivial example of frustration is realized in an one-dimensional Heisenberg chain with nearest neighbor ferromagnetic interaction $J_1 > 0$ and antiferromagnetic next-nearest neighbor interaction $J_2 < 0$, with $E = -\sum_n [J_1 \mathbf{S}_n \cdot \mathbf{S}_{n+1} + J_2 \mathbf{S}_n \cdot \mathbf{S}_{n+2}]$. If $|J_2| > J_1/4$ the ferromagnetic state becomes unstable and a spin-spiral state with a wave vector $\cos q = J_1/(4|J_2|)$ has the lowest energy. This model explains for example the helimagnetic state of the lanthanides displayed in Fig. 5. For more information on the spin-spiral state see Eq. (45). Since the work of Heisenberg [49], the magnetism of complex spin structures of magnetic insulators has been almost exclusively discussed within the framework of model Hamiltonians, first and foremost the Heisenberg Hamiltonian, to which we refer in its classical version, replacing the Pauli matrices $(\sigma_x, \sigma_y, \sigma_z)$ with the $SU(2)$ symmetry by classical vectors S_x, S_y, S_z of $O(3)$ symmetry, neglecting the possibility of quantum fluctuations:

$$\mathcal{H}_{\text{2-spin}} = -\sum_{i,j} J_{ij}\, \mathbf{S}_i \cdot \mathbf{S}_j \qquad \text{and} \qquad \mathbf{S}_i^2 = S^2, \text{ for all } i\ , \tag{2}$$

i.e. the spins of the d-electrons localized on the lattice sites i, j are considered as classical vectors $\mathbf{S}$, with the assumption that the spins on all lattice sites have the same magnitude S. The exchange interaction between the spins is isotropic and described by the pair interaction J_{ij}. In localized model spin systems the J_{ij} can be safely approximated by the ferromagnetic ($J_1 > 0$) or antiferromagnetic ($J_1 < 0$) nearest-neighbor (n.n.) interaction, i.e. $J_{ij} = 0$ for all

i, j, except for $J_{n.n.} = J_1$. Although in magnetic insulators J_1 often dominates over the rest of the further distant pairs, an attempt to reproduce the magnetic complexity or the T_c solely from J_1 produces results of limited quality or often simply fails. In magnetic insulators the inclusion of several neighbors is important. Please notice, in the literature one finds a set of slightly different definitions of the Heisenberg model. I have chosen here a negative sign. Further, I have not corrected the double counting of sites $(i,\, j)$ and $(j,\, i)$ by a prefactor $1/2$.
In the Lecture B1 *Model Hamiltonians and Second Quantization* we have seen that the Heisenberg model, which is an effective spin-model, can be derived from the Hubbard model which describes the motion of electrons on the lattice at the presence of on-site electron correlation. Analogously, exchange interactions beyond the Heisenberg model can be motivated from a perturbation expansion of the Hubbard model [50] in powers of t^2/U in the limit of large U (see Eq. 32 of Lecture B1). Expanding the Hubbard model into a spin model, replacing the spin operators by classical spin vectors, a second order perturbation expansion reproduces the classical Heisenberg model with $J_1 = 2t^2/U$. J arises from the same kind of kinetic exchange process kinetic exchange process that we learned about in connection with the H_2 problem.
For itinerant transition-metal magnets and depending on the Fermi surfaces J_{ij} between distant pairs are required to model the properties with reliability. Distances up to the 10th nearest neighbor are not uncommon. In most cases also in transition-metal magnets the interaction between the 1^{st} neighbor is the largest.

2.2 Higher-order exchange

The fourth order perturbation treatment (the third order is zero in the absence of spin-orbit interaction) yields two additional terms of different form. One is the four-spin exchange interaction (4-spin):

$$\mathcal{H}_{\text{4-spin}} = \sum_{ijkl} K_{ijkl}\big[(\mathbf{S}_i\mathbf{S}_j)(\mathbf{S}_k\mathbf{S}_l) + (\mathbf{S}_j\mathbf{S}_k)(\mathbf{S}_l\mathbf{S}_i) - (\mathbf{S}_i\mathbf{S}_k)(\mathbf{S}_j\mathbf{S}_l)\big]\ . \tag{3}$$

The 4-spin interaction is so-called ring-exchange and arises from four consecutive hops of electrons from one spin configuration to the spin-flipped one. For the sake of simplicity let us consider a four-site ring with nearest neighbor hopping. Denoting the eigenstates as $|S_1^z S_2^z S_3^z S_4^z\rangle$, etc., we find for example

$$|\uparrow\downarrow\uparrow\downarrow\rangle \rightsquigarrow |0(\uparrow\downarrow)\uparrow\downarrow\rangle \rightsquigarrow |\downarrow\uparrow\uparrow\downarrow\rangle \rightsquigarrow |\downarrow\uparrow(\uparrow\downarrow)0\rangle \rightsquigarrow |\downarrow\uparrow\downarrow\uparrow\rangle\,. \tag{4}$$

Such a change is effected by $S_1^- S_2^+ S_3^- S_4^+$ (with e.g. $S_3^-|\uparrow\uparrow\uparrow\uparrow\rangle = |\uparrow\uparrow\downarrow\uparrow\rangle$). Since the total Hamiltonian is spin-rotationally invariant, this must be part of the isotropic term $(\mathbf{S}_1\mathbf{S}_2)(\mathbf{S}_3\mathbf{S}_4)$. By symmetry, the term $(\mathbf{S}_2\mathbf{S}_3)(\mathbf{S}_4\mathbf{S}_1)$ must have the same coefficient. Finally, we can convince ourselves that there must exist a term like $(\mathbf{S}_1\mathbf{S}_3)(\mathbf{S}_2\mathbf{S}_4)$ as well. An algebraic trick to facilitate the spin exchange between two sites i and j is to introduce the permutation operator (also known as Dirac spin-exchange operator [51], $\mathcal{P}_{ij} = 2(\mathbf{S}_i \cdot \mathbf{S}_j + 1/2)$ with $\mathcal{P}_{12}|\sigma_1\sigma_2\rangle = |\sigma_2\sigma_1\rangle$. Enumerating all the processes, one finds the four-site term $\mathcal{H}_{\text{4-spin}} = \sum_{ijkl} \mathcal{P}_{ij}\mathcal{P}_{jk}\mathcal{P}_{kl}\mathcal{P}_{li}$ (or plaquette exchange) [50] given in Eq. (3) with $K_{\text{n.n.}} = 5t^4/U^3$. This is strictly true only for systems with localized $S = 1/2$ spins. For $S > 1/2$ magnets (which may be described by degenerate Hubbard models), more possibilities have to be considered and the first non-trivial term, which appears is the biquadratic exchange:

$$\mathcal{H}_{\text{biquadr}} = \sum_{ij} B_{ij}(\mathbf{S}_i \cdot \mathbf{S}_j)^2\ . \tag{5}$$

The exchange parameters J_{ij}, K_{ijkl}, and B_{ij} depend on the details of the electronic structure, e.g. the Fermi surface in case of metals. Since the higher-order terms scale with the magnetic moment to 4th-order, their relative importance increases with increasing magnetic moments. They should therefore become important for Fe atoms and for transition-metals atoms at surfaces. Although the higher-order magnetic interactions are in general small may be 5% of J, their value lies in the fact that they can lift the degeneracy of those magnetic states that are degenerate in the Heisenberg model. Further, there is always a chance that they play a role in frustrated magnets, where the competition between leading-order terms leaves the questions of order for the weaker terms to decide [52, 53].

2.3 Dipole-dipole interaction

For completeness I would like to mention that a piece of magnetic material is typically magnetically anisotropic. This means that the total energy depends on the orientation of the magnetization as measured with respect to the crystal axes and the sample shape. Thus, besides the isotropic exchange interaction there are additional interactions, so-called anisotropic interactions. This orientation dependent energy contribution is called the *magnetic anisotropy energy* (MAE), $E_{\rm MAE}$. Without this effect of the magnetic anisotropy, magnetism would have been hard to discover and possibly useless. In some way or the other, almost all applications of magnetic materials hinge on the fact that it is easier to magnetize a magnetic material in one direction than another. The magnetic anisotropy is responsible for the occurrence of easy and hard axes. The magnetic anisotropy has two origins:
(i) one is the classical dipole-dipole interaction between magnetic moments of localized spins $\mathbf{M}$ at transition-metal sites.

$$\mathcal{H}_{\rm dip} = \sum_{i\neq j} \frac{1}{r_{ij}^3}(\mathbf{M}_i \cdot \mathbf{M}_j - 3(\mathbf{M}_i \cdot \hat{\mathbf{r}}_{ij})(\mathbf{M}_j \cdot \hat{\mathbf{r}}_{ij}))\,, \tag{6}$$

where $\hat{\mathbf{r}}_{ij}$ is the unit vector pointing in the direction of $\mathbf{r}_j - \mathbf{r}_i = \mathbf{r}_{ij}$. It is worth mentioning that $\mathbf{M}$ is the total magnetic moment of the ion including the orbital magnetic contribution. Thus, the effect of the dipole-dipole interaction will be relatively strong for rare-earth ions ($\mathbf{M} \propto \mathbf{J} = \mathbf{L} + \mathbf{S}$), while for $3d$ transition-metal magnets and transition-metal oxides, $\mathbf{M} \propto \mathbf{S}$. For antiferromagnets the contribution is zero or very small (in case of weak ferromagnetism due to e.g. Dzyaloshinskii-Moriya interaction). Due to the long range nature of the dipole-dipole interaction it contributes mostly to the *shape anisotropy* of the MAE.

2.4 Anisotropy of on-site interaction

(ii) The second contribution arises from the spin-orbit coupling,

$$\mathcal{H}_{\rm SO} = \xi\, \mathbf{L} \cdot \mathbf{S}\,, \tag{7}$$

leaving a degeneracy $(2|\mathbf{J}| + 1)$, which relates the spin-degree of freedom to the motion of the electrons in the lattice and contributes exclusively to the *magneto-crystalline anisotropy* (MCA). Its strength depends crucially on the symmetry of the lattice and the orbital moment in the crystal. It is frequently called the *single-ion anisotropy*.
In crystal field theory we learn that the crystal field Hamiltonian is described by a real potential, enabling the choice angular wavefunctions usinging only real numbers. Thus, one may choose

eigenstates which are also real. Since the angular momentum is a purely imaginary operator, it implies that for such an eigenstate:

$$\langle\psi|\mathbf{L}|\psi\rangle = 0\,, \tag{8}$$

i.e. angular momentum is quenched, and only the spin degree of freedom remains. There is however a caveat if the crystal field does not entirely remove the degeneracies, then from a pair of degenerate real wavefunctions, one may construct combinations for which the above equality does not hold. In magnetic insulators it is usually such that degeneracies do not survive, since it becomes energetically more favorable to pay the (quadratic) elastic cost of deforming a symmetric lattice to gain a linear decrease in electronic energy from splitting a degenerate state. Assuming complete quenching of angular momentum, i.e. $\langle\psi|\mathbf{L}|\psi\rangle = 0$, it is clear that the spin-orbit perturbation at site i, $\mathcal{H}_{\rm SO}(i) = \xi\,\mathbf{L}_i \cdot \mathbf{S}_i$ has no effect at first order in perturbation theory, as there is no remaining degeneracy to break. However, this term may still have an effect in second (and higher) order perturbation theory. Considering an unknown spin state, but integrating out orbital excitations perturbatively, one may write:

$$\mathcal{H}^{(2)}_{\rm MCA} = \delta H = |\xi|^2 \sum_n \frac{\langle 0|L_\mu|n\rangle\langle n|L_\nu|0\rangle}{E_0 - E_n} S_{\mu\nu} = -S_\mu \Lambda_{\mu\nu} S_\nu\,, \tag{9}$$

where μ, ν run over the three cartesian components x, y, z and generally $\Lambda_{\mu\nu}$ is not proportional to the identity matrix, but depends on the ordering of the excited orbitals. Rotating the real, symmetric 3×3 tensor into the principle axes Λ is conventionally written as $\Lambda_{\mu\mu} = K_{2\mu}\delta_{\mu\mu}$, with $K_2 \propto |\xi|^2$ and the uniaxial anisotropy at all sites i is summarized to

$$\mathcal{H}^{(2)}_{\rm MCA} = \sum_i K_{2;ix} S^2_{i,x} + K_{2;iy} S^2_{i,y} + K_{2;iz} S^2_{i,z}. \tag{10}$$

This equation holds for transition-metal atoms with a two fold symmetry in all three directions. This is a rare case. Frequently, transition-metal ions are located in a cubic or octahedral environment. Then all terms in second order perturbation theory are zero and the first nonvanishing contribution result from the 4th order perturbation theory. The magnetic anisotropy changes to

$$\mathcal{H}^{(4)}_{\rm MCA} = \sum_i K_{4;i}\,(S^4_{i,x} + S^4_{i;y} + S^4_{i,z})\,, \tag{11}$$

with an anisotropy strength $K_4 \propto |\xi|^4$. This contribution is small. Frequently, the system has a Jahn-Teller distortion, that lowers the symmetry and then a second order contribution is added with an additional smallness parameter, the displacement of the atom that breaks the symmetry.

2.5 Antisymmetric exchange: Dzyaloshinskii-Moriya interaction

In 1957 Dzyaloshinskii [20] predicted on the basis of symmetry arguments the presence of a unidirectional magnetic interaction of the form:

$$\mathcal{H}_{\rm DM} = \sum_{i,j} \mathbf{D}_{ij} \cdot (\mathbf{S}_i \times \mathbf{S}_j)\ , \tag{12}$$

where the Dzyaloshinskii-vector, $\mathbf{D}$, is a vector, which depends on the symmetry of the system and on the real space direction given by two sites i and j. The presence of the DM interaction has far-reaching consequences. Depending on the sign, the symmetry properties, and the

value of the Dzyaloshinskii vector $\mathbf{D}_{ij}$, collinear uniaxial ferro- or antiferromagnetic structures are becoming unstable and are instead replaced by a directional noncollinear magnetic structure of one specific chirality, $\mathbf{c} = \mathbf{S}_i \times \mathbf{S}_{i+1}$, either a right-handed ($c > 0$) or left-handed ($c < 0$) one. The interaction is fundamentally different to the direct, kinetic, or metallic exchange interactions we have been discussed before that are caused exclusively by the Coulomb interaction. Those are symmetric, i.e. two magnetic configurations with right-handed ($\nwarrow\nearrow$) or left-handed ($\nearrow\nwarrow$) alignment of the magnetic moments have the same energy. The nature of the DM interaction prefers non-collinear magnetic structures and is responsible for weak ferromagnetism, i.e. the occurrence of small net magnetic moments of otherwise antiferromagnetic materials. In this context one may think of hematite (Fe_2O_3), a mineral with an antiferromagnet exchange ($J > 0$) as an example. The canting angle can be estimated from a simple two-site model

$$\mathcal{H}_{\rm DM} = -J\mathbf{S}_1 \cdot \mathbf{S}_2 \; + \; \mathbf{D} \cdot (\mathbf{S}_1 \times \mathbf{S}_2) \; .$$

Assuming that the spins $\mathbf{S}_1$ and $\mathbf{S}_2$ are placed in the same plane, then the energy depends only on the angle θ between the spins ($\searrow\swarrow$)

$$E = -JS^2 \cos\theta + DS^2 \sin\theta \; ,$$

with the canting angle $\tan(\pi - \theta_{\rm min}) = -D/J$. $\mathcal{H}_{\rm DM}$ has the most general form of an antisymmetric tensor of 2$^{\rm nd}$ rank which is second order in spin $\mathbf{S}$. Typically, the combination of hopping of spin-polarised electrons and the presence of spin-orbit interaction can produce such a term. The microscopic details depend on the solid and are described in different microscopic models. In my opinion the minimal model to obtain an antisymmetric exchange interaction consists of 3 atoms, whereby at least two of which are magnetic and and one of which carries spin-orbit interaction. The most famous one is the model of Moriya explaining the DM interaction in magnetic insulators. He derived also rules under which circumstances the DM interaction will occur. These rules are general and should apply also to metallic systems.

Magnetic Insulators: Moriya [21] explained the origin of the interaction for transition-metal oxides on the basis of a microscopic picture, which combines the kinetic (super-)exchange due to hopping electrons that would be described by the Heisenberg model, with the *on-site* spin-orbit coupling at each site that we have discussed in Section 2.4, giving rise to virtual excitations between the ground state g and excited states n. That is, why this interaction carries both names today and is called the *Dzyaloshinskii-Moriya interaction*. It is also referred to as *antisymmetric exchange* or *antisymmetric superexchange*. We discuss this here on the basis of a small two-site model and consider:

$$H = \xi\, \mathbf{L}_1 \cdot \mathbf{S}_1 \; + \; \xi\, \mathbf{L}_2 \cdot \mathbf{S}_2 \; + \; \hat{J}\mathbf{S}_1 \cdot \mathbf{S}_2 \tag{13}$$

where $\hat{J}$ is an operator that depends on what orbital state the electron is in; at the ground state g or at one of the excited states n. Normally this fact is irrelevant because the orbital states are split, and so one may normally consider $\hat{J} \to J = \langle 0|J|0\rangle$, but combined with the spin-orbit coupling we may write consistent with the schematic picture of the hopping paths of the electrons given in Fig. 10:

$$\mathcal{H}_{\rm DM} = \delta H = -\xi \sum_{n_1} \left[\frac{\langle g_1 g_2|\mathbf{L}_1 \cdot \mathbf{S}_1|n_1 g_2\rangle\langle n_1 g_2|\hat{J}\mathbf{S}_1 \cdot \mathbf{S}_2|g_1 g_2\rangle}{E_{n_1 g_2} - E_{g_1 g_2}} \right. \tag{14}$$

$$\left. + \; \frac{\langle g_1 g_2|\hat{J}\mathbf{S}_1 \cdot \mathbf{S}_2|n_1 g_2\rangle\langle n_1 g_2|\mathbf{L}_1 \cdot \mathbf{S}_1|g_1 g_2\rangle}{E_{n_1 g_2} - E_{g_1 g_2}} \right] + (1 \Leftrightarrow 2).$$

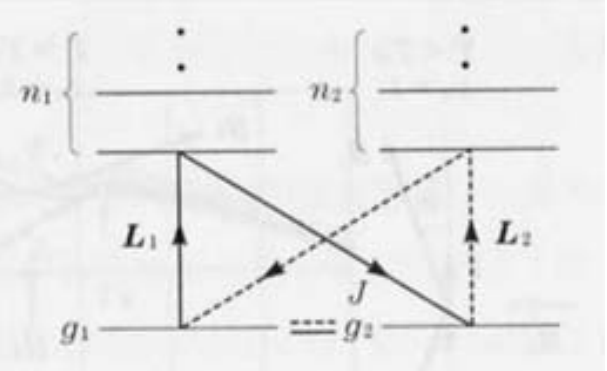

Fig. 10: *Interaction channels of hopping electrons that give rise to the Dzyaloshinskii-Moriya interaction.*

This may be simplified because, for real wavefunctions one has $\langle g_1|\mathbf{L}_1|n_1\rangle = \langle n_1|\mathbf{L}_1|g_1\rangle^* = -\langle n_1|\mathbf{L}_1|g_1\rangle$ and $\langle n_1 g_2|\hat{J}|g_1 g_2\rangle = J(n_1 g_2|g_1 g_2) = J(g_1 g_2|n_1 g_2) = \langle g_1 g_2|\hat{J}|n_1 g_2\rangle$, hence

$$\mathcal{H}_{\rm DM} = -2\xi \sum_{n1} \frac{\langle g_1|\mathbf{L}_1|n_1\rangle\langle n_1 g_2|\hat{J}|g_1 g_2\rangle}{E_{n_1 g_2} - E_{g_1 g_2}} [\mathbf{S}_1, \mathbf{S}_1 \cdot \mathbf{S}_2] \; + \; (1 \Leftrightarrow 2). \tag{15}$$

Writing the sum over n_1 as D_1, and using the commutation relations to write, $[\mathbf{S}_1, \mathbf{S}_1 \cdot \mathbf{S}_2] = -i\mathbf{S}_1 \times \mathbf{S}_2$ and $[\mathbf{S}_2, \mathbf{S}_1 \cdot \mathbf{S}_2] = i\mathbf{S}_2 \times \mathbf{S}_1$ one can write

$$\mathcal{H}_{\rm DM} = (\mathbf{D}_1 - \mathbf{D}_2) \cdot (\mathbf{S}_1 \times \mathbf{S}_2) \;\; , \quad \text{with} \quad \mathbf{D}_1 = -2i\,\xi \sum_{n1} \frac{\langle g_1|\mathbf{L}_1|n_1\rangle}{E_{n_1 g_2} - E_{g_1 g_2}} J(n_1 g_2|g_1 g_2) \tag{16}$$

The strength of the Dzyaloshinskii-Moriya interaction, i.e. the length of the Dzyaloshinskii-vector, respectively, can be estimated to $D \approx |\frac{\xi}{\Delta E}|J$, and is thus first order in the spin-orbit interaction, in difference to the single-ion anisotropy (Section 2.4) that is at least second order. It is thus clear, that D is equal zero, $D = 0$, in case of a mirror symmetry or point of inversion between the two atoms. In other words, the DM interaction exists only between two *different* atoms. However, *different* need not mean different species of ion, but can just mean different chemical environments, such as in a bipartite lattice, where the symmetry of orbitals may be different between the two types of lattice site. In article [21], Moriya derived the following symmetry rules (also expressed schematically in Fig. 11: Considering two ions located at sites A and B, respectively, and the point bisecting the straight line AB is denoted by C. The rules are:

(i) When a center of inversion is located at C: $\mathbf{D} = 0$.

(ii) When a mirror plane perpendicular to AB passes through C: $\begin{cases} & \mathbf{D} \parallel \text{mirror plane} \\ \text{or} & \mathbf{D} \perp AB. \end{cases}$

(iii) When there is a mirror plane including A and B: $\mathbf{D} \perp$ mirror plane.

(iv) When a two-fold rotation axis perpendicular to AB passes through C: $\mathbf{D} \perp$ two-fold axis

(v) When there is an n-fold ($n \geq 2$) along AB: $\mathbf{D} \parallel AB$

The DM interaction plays an important role in the field of multiferroics. It is one of the possible interactions that causes a linear magnetoelectric effect, $\Phi = -\alpha_{ij} E_i B_J$, with the electric polarization $P_i = -\partial\Phi/\partial E_i = \alpha_{ij} B_j$ and the magnetization $M_i = -\partial\Phi/\partial B_i = \alpha_{ji} E_j$ coupling.

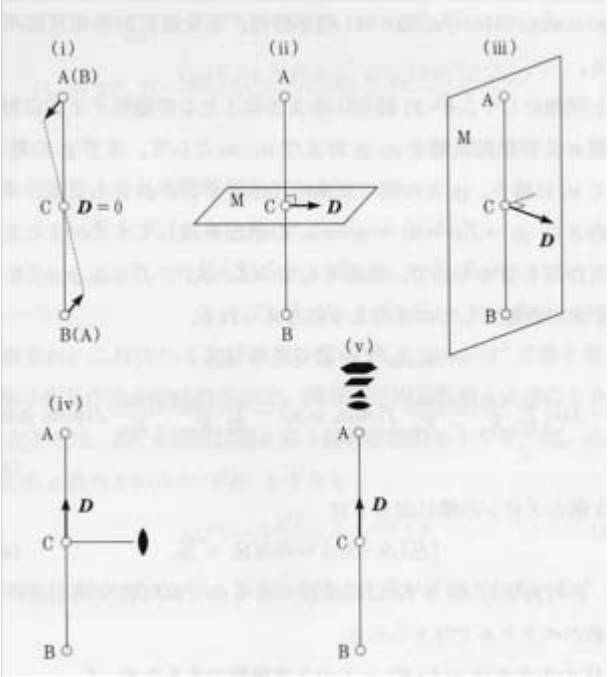

Fig. 11: *Direction of the Dzyaloshinskii-Moriya vector for a diatomic molecules located at sites A and B according to the symmetry rules of Moriya [21].*

An example is Cr_2O_3. The DM interaction causing magnetic structures with a unique rotational order – we think in particular at cycloidal spirals $\mathbf{M} = M(\hat{\mathbf{x}}\cos\mathbf{qR} + \hat{\mathbf{y}}\sin\mathbf{qR})$, $\mathbf{R} \perp (\hat{\mathbf{x}}\hat{\mathbf{y}})$ – can also be a source of inversion symmetry breaking in a structurally symmetric compound being the origin of magnetic ferroelectrics also known as improper multiferroelectrics [54]. In such spirals ferroelectric polarization P is introduced that is proportional to the outer product of $\mathbf{P} \propto [\hat{\mathbf{z}} \times \mathbf{q}_x]$. In these systems the magnetoelectric coupling is rather strong. This new class of materials include for example $TbMnO_3$, $TbMn_2O_5$, $Ni_3V_2O_8$, $MnWO_4$, $CoCr_2O_4$, $CuFeO_2$ etc..

Magnetic Metals: The antisymmetric spin-interaction in metals had been discussed in different microscopic models that go back to Smith [55], Fert and Levy [56, 57] and the Kanamori-group [58]. Fert and Levy [56] derived an expression for this anisotropic exchange interaction of two magnetic atoms in spin-glasses doped with heavy impurity atoms, i.e. impurity atoms with a large nuclear number and thus a large spin-orbit interaction, which is of the form

$$\mathcal{H}_{\rm DM} = -V(\xi)\frac{\sin\left[k_{\rm F}(R_A + R_B + R_{AB}) + \eta\right]\hat{\mathbf{R}}_A \cdot \hat{\mathbf{R}}_B}{R_A R_B R_{AB}}(\hat{\mathbf{R}}_A \times \hat{\mathbf{R}}_B)(\mathbf{S}_A \times \mathbf{S}_B) \qquad (17)$$

where $\mathbf{R}_A = R_A\hat{\mathbf{R}}_A$ and $\mathbf{R}_B = R_B\hat{\mathbf{R}}_B$ are the positions of the magnetic atoms measured from the nonmagnetic impurity and R_{AB} is the distance between the atoms A and B. $V(\xi)$ is a term that depends of the spin-orbit coupling constant of the nonmagnetic atom, ξ, $k_{\rm F}$ is the Fermi vector and η the phase shift induced by the impurity. The sinus term reflects the RKKY-type character of the interaction, while the two cross products determine the symmetry of the interaction. How far this model holds for real materials has not thoroughly been investigated yet on the basis of density functional theory. The model should be also applicable to adatoms on surfaces. Here, Rashba electrons, electrons in a surface state that is subject to the presence

of spin-orbit interaction as well as the structure inversion asymmetry due to the presence take the role of the heavy atoms and produce also an antisymmetric exchange interaction, which has recently been investigated by Bouaziz *et al.* [59], which is proportional to the Rashba strength and falls off with a slower power law that is $1/R^2$ or $1/R$ for large distances.
At the end we summarise all spin-spin interactions, due to exchange with and without spin-orbit interaction, that can be described up to second order by the Hamiltonian

$$H = \sum_i K(\mathbf{S}_i) + \sum_{ij(i\neq j)} \mathbf{S}_i \mathsf{J}_{ij} \mathbf{S}_j \tag{18}$$

Here, the first term describes the on-site anisotropy energy and the second term (where $i \neq j$) includes the intersite exchange interactions and the Dzyaloshinskii-Moriya interaction. The quantities J_{ij} are 3×3 matrices (second rank tensors in real space). They can be decomposed in symmetric and antisymmetric parts as: $\mathsf{J}_{ij} = J_{ij}1 + \mathsf{J}^{\mathrm{S}}_{ij} + \mathsf{J}^{\mathrm{A}}_{ij}$ with J_{ij} being the usual Heisenberg exchange interaction $J_{ij} = 1/3\,\mathrm{Tr}\mathsf{J}_{ij}$, $\mathsf{J}^{\mathrm{S}}_{ij}$ the *anisotropic exchange interaction* or sometimes called two-ion anisotropy which is the (traceless) symmetric part $\mathsf{J}^{\mathrm{S}}_{ij} = \frac{1}{2}\left(\mathsf{J}_{ij} + \mathsf{J}^{t}_{ij}\right) - J_{ij}1$, and $\mathsf{J}^{\mathrm{A}}_{ij}$ the antisymmetric part: $\mathsf{J}^{\mathrm{A}}_{ij} = \frac{1}{2}\left(\mathsf{J}_{ij} - \mathsf{J}^{t}_{ij}\right)$. The latter can be brought in connection with the Dzyaloshinskii-Moriya interaction constants via the antisymmetric tensor, $D^x_{ij} = \varepsilon_{xyz} J^{\mathrm{A}yz}_{ij}$, and the spin-spin interaction in its general form is then written in terms of the Dzyaloshinskii-Moriya vectors as

$$\mathbf{S}_i \mathsf{J}_{ij} \mathbf{S}_j = J_{ij}\mathbf{S}_i\mathbf{S}_j + \mathbf{S}_i \mathsf{J}^{\mathrm{S}}_{ij} \mathbf{S}_j + \mathbf{D}_{ij}(\mathbf{S}_i \times \mathbf{S}_j). \tag{19}$$

Above not much has been said about the anisotropic exchange interaction. It is second order in spin-orbit interaction, while the Dzyaloshinskii-Moriya interaction is first order. It is important to notice that all these exchange interactions and those beyond the simple models discussed here are included (in many case to high accuracy) in density functional theory, which we describe next, although there one-to-one correspondence it not always trivial.

3 Spin Density Functional Theory

In 1964 Hohenberg and Kohn [60] worked out two central theorems that form the basis of density functional theory (DFT): For a system of N particles (e.g. electrons) moving in an external potential $v(\mathbf{r})$ (caused by e.g. nuclei) in a non-degenerate ground state (i) the many-body wavefunction Ψ and $v(\mathbf{r})$ are uniquely determined by the particle density distribution $n(\mathbf{r})$ and (ii) there exists an energy functional of this density, $E[n(\mathbf{r})]$, which is stationary with respect to variations of the ground-state density. These two theorems allow – at least in principle – the determination of the ground-state density and energy of a N-particle system. Extracting the classical Coulomb interaction energy, such a Hohenberg-Kohn energy functional takes the form

$$E[n(\mathbf{r})] = \int v(\mathbf{r}) n(\mathbf{r}) d\mathbf{r} + \frac{1}{2}\int\int \frac{n(\mathbf{r})n(\mathbf{r}')}{|\mathbf{r}-\mathbf{r}'|} d\mathbf{r} d\mathbf{r}' + G[n(\mathbf{r})] \tag{20}$$

where the functional $G[n(\mathbf{r})]$ has to be approximated.
In the Kohn-Sham theory [61], the kinetic energy T_0 of a non-interacting electron gas in its ground state with a density distribution $n(\mathbf{r})$ is further extracted from $G[n(\mathbf{r})]$, so that a new functional

$$E_{\mathrm{xc}}[n(\mathbf{r})] = G[n(\mathbf{r})] - T_0[n(\mathbf{r})] \tag{21}$$

remains to be determined. $E_{\rm xc}$ is now called exchange-correlation energy functional, since without $E_{\rm xc}$ our energy functional E would yield just the Hartree energy. If we take into account that particle conservation, i.e. $N = \int n(\mathbf{r})d\mathbf{r}$ has to be ensured, we can formulate the stationarity of E in Eq. (20) with respect to variations of the ground-state density as

$$v(\mathbf{r}) + \int \frac{n(\mathbf{r}')}{|\mathbf{r}-\mathbf{r}'|}d\mathbf{r}' + \frac{\delta T_0}{\delta n(\mathbf{r})} + \frac{\delta E_{\rm xc}}{\delta n(\mathbf{r})} - \lambda = 0 \tag{22}$$

where the Lagrange parameter λ ensures the particle conservation. Expressing the kinetic energy of the non-interacting particles via their wavefunctions, ϕ_i, we can recast Eq. (22) in the form of an effective single particle Schrödinger equation:

$$\left[-\frac{\hbar^2}{2m}\nabla^2 + v(\mathbf{r}) + \int \frac{n(\mathbf{r}')}{|\mathbf{r}-\mathbf{r}'|}d\mathbf{r}' + \frac{\delta E_{\rm xc}}{\delta n(\mathbf{r})}\right]\phi_i(\mathbf{r}) = \epsilon_i\phi_i(\mathbf{r}) \tag{23}$$

which has to be solved self-consistently since $n(\mathbf{r}) = \sum_{i=1}^{N}|\phi_i(\mathbf{r})|^2$. The last term of the Hamiltonian is called the exchange-correlation potential. For more detailed information see Lecture A2 *Introduction to Density Functional Theory*.

3.1 The density and potential matrix

In 1972 von Barth and Hedin extended this concept to spin-polarized systems [62], replacing the scalar density by a hermitian 2×2 matrix $\mathsf{n}(\mathbf{r})$. If $\psi_\alpha(\mathbf{r})$ is the field operator for a particle of spin α, a component of the spin-density matrix can be defined as

$$n_{\alpha\beta}(\mathbf{r}) = \langle\Psi|\psi^+_\beta(\mathbf{r})\psi_\alpha(\mathbf{r})|\Psi\rangle. \tag{24}$$

The potential matrix corresponding to this spin-density matrix is denoted as $\mathsf{v}(\mathbf{r})$ and replaces the scalar potential. Then, we can write Eq. (23) in the form

$$\left[\left(-\frac{\hbar^2}{2m}\nabla^2 + \sum_\alpha\int\frac{n_{\alpha\alpha}(\mathbf{r}')}{|\mathbf{r}-\mathbf{r}'|}d\mathbf{r}'\right)\mathsf{I} + \mathsf{v}(\mathbf{r}) + \frac{\delta E_{\rm xc}}{\delta\mathsf{n}(\mathbf{r})}\right]\begin{pmatrix}\phi_i^{(+)}(\mathbf{r})\\ \phi_i^{(-)}(\mathbf{r})\end{pmatrix} = \epsilon_i\begin{pmatrix}\phi_i^{(+)}(\mathbf{r})\\ \phi_i^{(-)}(\mathbf{r})\end{pmatrix} \tag{25}$$

where I is a 2×2 unit matrix and the exchange-correlation potential, v, is now also a 2×2 matrix. In terms of the Kohn-Sham wavefunctions, the density matrix can now be written as

$$n_{\alpha\beta}(\mathbf{r}) = \sum_{i=1}^{N}\phi_i^{*\alpha}(\mathbf{r})\phi_i^{\beta}(\mathbf{r}) \quad \text{where} \quad \alpha,\beta = (+),(-). \tag{26}$$

Using the Pauli matrices, $\boldsymbol{\sigma}$, the density matrix can be decomposed in a scalar and a vectorial part, corresponding to the charge and magnetization density:

$$\mathsf{n}(\mathbf{r}) = \frac{1}{2}\left(n(\mathbf{r})\mathsf{I} + \boldsymbol{\sigma}\cdot\mathbf{m}(\mathbf{r})\right) = \frac{1}{2}\begin{pmatrix} n(\mathbf{r})+m_z(\mathbf{r}) & m_x(\mathbf{r})-im_y(\mathbf{r})\\ m_x(\mathbf{r})+im_y(\mathbf{r}) & n(\mathbf{r})-m_z(\mathbf{r})\end{pmatrix}. \tag{27}$$

Likewise, the potential matrices can be written in terms of a scalar potential and magnetic field, $\mathbf{B}(\mathbf{r})$:

$$\mathsf{v}(\mathbf{r}) = v(\mathbf{r})\mathsf{I} + \mu_B\boldsymbol{\sigma}\cdot\mathbf{B}(\mathbf{r}) \quad \text{and} \quad \mathsf{v}_{\rm xc}(\mathbf{r}) = v_{\rm xc}(\mathbf{r})\mathsf{I} + \mu_B\boldsymbol{\sigma}\cdot\mathbf{B}_{\rm xc}(\mathbf{r}) \tag{28}$$

where $\mu_{\rm B} = \frac{e\hbar}{2mc}$ is the Bohr magneton.

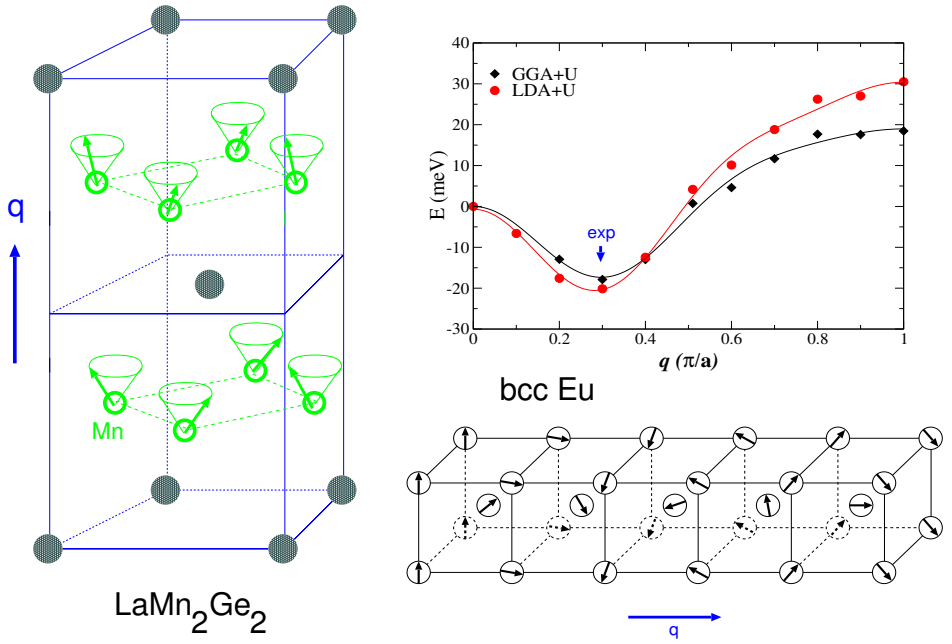

Fig. 12: *Examples of non-collinear ground-states: in $LaMn_2Ge_2$ the spins on the Mn sublattice can be described by a conical spin-spiral, i.e. the magnetization precesses on a cone with a semicone-angle of* $58°$ *from layer to layer in* z*-direction. The turning angle per layer is* $128°$*. The magnetic structure is in good agreement with first-principles calculations [63]. Bulk bcc europium has a flat spiral in* $[001]$ *direction as ground state (right, bottom), the length of the* $\mathbf{q}$*-vector, describing this precession, is correctly reproduced by DFT [64] (right, top).*

Within this formalism, general non-collinear structures can be described in the framework on density functional theory. Two recent examples, $LaMn_2Ge_2$ and bcc-Eu, are shown in Fig. 12.

Numerically, Eq. (25) is solved by expanding $\phi_i(\mathbf{r})$ in a linear combination of suitable basis-functions $\chi_j(\mathbf{r})$. Then Eq. (25) transforms into a eigenvalue problem and the eigenvectors, that have to be determined, give the linear combination coefficients, c_{ij}, of the expansion $\phi_i(\mathbf{r}) = \sum_j c_{ij}\chi_j(\mathbf{r})$. Such an eigenvalue problem is a standard problem of linear algebra and the computational effort scales in the most general case with the third power of the number of basis-functions. Compared to the non-magnetic problem, Eq. (23), this number is doubled in Eq. (25). Therefore, the computational effort for a general, non-collinear calculation is increased by a factor eight as compared to the non-magnetic calculation. An additional factor of at least 2 comes from the fact that the Hamiltonian is now hermitian and not anymore symmetric and another factor of about 4 can easily come in since the non-collinear magnetism reduces the symmetry and a larger irreducible part of the Brillouine-zone has to be sampled.

3.2 The collinear case

Supposing that the potential matrices in Eq. (28) are diagonal (i.e. the magnetic and exchange fields point in z direction), Eq. (25) decouples into two equations of the type of Eq. (23):

$$\left(-\frac{\hbar^2}{2m}\nabla^2 + v_{\rm Coul}(\mathbf{r}) + v(\mathbf{r}) + B_z(\mathbf{r}) + v_{\rm xc}^{(+)}(\mathbf{r})\right)\phi_i^{(+)}(\mathbf{r}) = \epsilon_i^{(+)}\phi_i^{(+)}(\mathbf{r}) \quad (29)$$
$$\left(-\frac{\hbar^2}{2m}\nabla^2 + v_{\rm Coul}(\mathbf{r}) + v(\mathbf{r}) - B_z(\mathbf{r}) + v_{\rm xc}^{(-)}(\mathbf{r})\right)\phi_i^{(-)}(\mathbf{r}) = \epsilon_i^{(-)}\phi_i^{(-)}(\mathbf{r})$$

where $v_{\rm Coul}$ denotes now the classical Coulomb potential and $v_{\rm xc}^{(+,-)}$ the exchange-correlation potential that arises from the functional derivative of the exchange-correlation energy with respect to the spin-up $(+)$ or spin-down $(-)$ part of the diagonal density matrix.
Since the two equations (29) can be solved independently, the computational effort for a collinear calculation seems to be just twice the effort for a non-magnetic calculation. However, most magnetic calculations are computationally considerably more demanding since the quantities in question (magnetic moments, energy differences between various magnetic configurations) require much higher accuracy than what is needed for nonmagnetic systems. To explore different magnetic orders in a system, unit cells much larger than the chemical unit cell are required, e.g. antiferromagnetic body-centered cubic (bcc) chromium requires a calculation with at least two atoms in the unit cell (as compared to one, in a nonmagnetic calculation).
Systems that can be described by Eq. (29) are all kinds of magnetic materials that assume a collinear magnetic order, e.g. ferromagnetic, antiferromagnetic or ferrimagnetic states. Like the density is a property that can – at least in principle – be obtained exactly in DFT, the spin density is a property that is well defined in spin-polarized DFT:

$$\mathbf{m}(\mathbf{r}) = -\mu_{\rm B}\sum_{\alpha,\beta}\psi_\alpha^+(\mathbf{r})\boldsymbol{\sigma}_{\alpha\beta}\psi_\beta(\mathbf{r}). \quad (30)$$

The integral spin moment, M, for a collinear system is then (in units of $\mu_{\rm B}$) simply

$$M_{\rm spin} = \int m(\mathbf{r})d\mathbf{r} = \mu_{\rm B}\int \left(n^{(+)}(\mathbf{r}) - n^{(-)}(\mathbf{r})\right)d\mathbf{r}. \quad (31)$$

How well this quantity corresponds to experimental values depends of course on the quality of the exchange-correlation potential that is used for an actual calculation. Some examples of results obtained in the local spin density approximation (LSDA) and generalized gradient approximation (GGA) of (spin)-moments of elemental ferromagnets are given in Table 1.
The success of DFT calculations for magnetic systems – as shown in Table 1 – has to be contrasted here with the case of Cr, where up to now no satisfactory agreement with experimental results was obtained: while LSDA calculations of antiferromagnetic Cr at the experimental lattice constant give a magnetic moment in nice agreement with experimental data ($0.5 - 0.6\mu_{\rm B}$), calculations at the lattice constant determined with LSDA (which is 3% too small) yield a nonmagnetic ground state. GGA calculations, on the other hand, give a reasonable lattice constant, but the magnetic moment is more than 60% too large [65]. Also attempts to include the experimentally observed incommensurate sinusoidal modulation of the antiferromagnetic structure of Cr could nor resolve these discrepancies so far.
At this point we should notice, that we relied on the assumption that the total energy is invariant with respect to a uniform rotation of the magnetization direction. This was implicitly assumed when we arbitrarily (or, better, for convenience) selected in Eq. (29) the z direction as global magnetization axis. Indeed, in absence of an external field (or in its presence, as long as it is oriented in z direction) this implies no loss in generality, if $v_{\rm xc}$ is isotropic in space. If we start

Table 1: *Magnetic moments (in μ_B per atom) of ferromagnetic elements in the bulk. The experimentally determined total magnetization, $M_{tot.}$, consists of spin- and orbital moment contributions. The LSDA results for Fe, Co and Ni are taken from Moruzzi et al. [66], the GGA values from Shallcross and coworkers [67] where also experimental values are quoted. The calculated Gd data is from Kurz et al. [68], the experimental one from White and coworkers [69].*

Property	source	Fe (bcc)	Co (fcc)	Ni (fcc)	Gd (hcp)
M_{spin}	LSDA	2.15	1.56	0.59	7.63
M_{spin}	GGA	2.22	1.62	0.62	7.65
M_{spin}	experiment	2.12	1.57	0.55	
$M_{tot.}$	experiment	2.22	1.71	0.61	7.63

from a Schrödinger-Pauli like theory, there is indeed no term that could couple the spin-space to the lattice. Only if a spin-orbit coupling term (from a Dirac type theory) or – in some cases – dipolar interaction is included, a preferential direction for the collinear magnetization exists. This will be discussed in the next section.

3.3 Orbital magnetism

The magnetization density we discussed in the last section, Eq. (30), is clearly a consequence of the imbalance of electrons with spin-up or spin-down and, therefore, the quantity defined in Eq. (31) is called spin-moment. From atomic physics we know, that the total magnetic moment is a sum of spin- and orbital contributions, $M_{tot.} = M_{spin} + M_{orb}$. The orbital moment results, in a classical picture, from the orbital motion of the electron around the nucleus. Compared to the situation in a free atom, where M_{orb} can be even larger than M_{spin}, in a solid this motion is of course restricted by the crystal field that quenches the orbital moment. In bulk samples small moments (typically $0.1 - 0.2\mu_B$) can be found (compare Table 1).
Density functional theory in the known LSDA or GGA formulations provides no term that could lead to the formation of an orbital moment. Current- and spin-density functional theory [70] would provide a natural starting point for the description of orbital magnetism, but so far the successes are limited. From relativistic quantum mechanics [71], a two-component approximation to the Dirac equation can be formulated, that has the form of Eq. (25). From the several terms appearing in this Pauli equation one term, the spin-orbit coupling term, provides a mechanism that leads to orbital polarization: The electron, traveling on a classical trajectory around the nucleus, experiences the electric field (from the screened nucleus) as a magnetic field. This field couples to the magnetic (spin) moment of the electron and, thus, leads to a preferential orientation of the orbital motion. Using the orbital angular moment operator $\mathbf{L} = \mathbf{r} \times \mathbf{p}$, we can write the spin-orbit coupling term in the vicinity of a nucleus with a radial potential $v(r)$ as:

$$H_{so} = \frac{1}{r}\frac{dv(r)}{dr}(\boldsymbol{\sigma} \cdot \mathbf{L}). \tag{32}$$

Adding this term to Eq. (25) will destroy a decoupling of spin-up and -down equations like in Eq. (29). It also invalidates the aforementioned assumption that the total energy is not affected by a uniform rotation of the spin directions, since now spin-space and lattice are coupled by Eq. (32).

The orbital magnetization can be defined in analogy to Eq. (30), expressed in single particle wavefunctions ϕ_i:

$$\mathbf{m}(\mathbf{r}) = -\mu_{\rm B} \sum_i \langle \phi_i | \mathbf{r} \times \mathbf{p} | \phi_i \rangle. \tag{33}$$

At a certain atom ν, the orbital moment $M_\nu^{\rm orb}$ can then be obtained by an integration in a sphere centered around this atom:

$$M_\nu^{\rm orb} = -\mu_{\rm B} \sum_i \langle \phi_i | \mathbf{L} | \phi_i \rangle_\nu. \tag{34}$$

While this definition of the orbital moment poses no difficulties in periodic solids, we note here that the evaluation of the total orbital moment of a periodic crystal is more involved [72]. In most cases, however, the atomic orbital moments and also the magnetic anisotropy energies, obtained in density functional theory calculations, are too small as compared to experiment. Practical methods that can overcome this deficiency have been discussed in the literature [73].
Since the crystal field in a solid forces the orbital motion of the electron in a preferred plane, a total energy difference arises when the solid is magnetized in two different directions [74]. This difference, magnetocrystalline anisotropy energy (MAE), is small for bulk systems with high symmetry, e.g. cubic crystals like Fe or Ni. It is larger for crystals with a unique crystallographic axis, like hexagonal Co. But for lower dimensional systems, thin films or atomic wires, the magnetocrystalline anisotropy will essentially determine the magnetic properties, especially at finite temperatures [75].
The computational effort for calculations that include the spin-orbit coupling term, Eq. (32), can be reduced if this term is considered as a small perturbation to the non-relativistic Schrödinger-Pauli Hamiltonian. Then, the so-called magnetic force theorem [76] can be used to evaluate quantities like the MAE. But even these calculations require considerable computational resources, since the energy differences to be determined are very small and – compared to normal calculations – drastically increased numerical cutoffs can be necessary. Systems, where spin-orbit coupling is strong require a self-consistent treatment including Eq. (32) in the Hamiltonian. There, of course, the relativistic effects are stronger so that moderate numerical cutoffs can be used, but the computational complexity brought by the spin-orbit coupling term and the loss of symmetry that can be exploited leads to an increased computational effort.

4 The magnetic ground state

To determine the magnetic ground state it is possible to follow several directions: like in molecular-dynamics calculations, spin-dynamics allows to study the magnetic degrees of freedom exploring the ground state configuration. Another possibility is to determine the magnetic interactions between the atoms by a DFT calculation which are then mapped onto a model (in the simplest case a classical Heisenberg model). This model is then solved, either analytically or numerically. In both cases we introduce a discretization of the (vector) magnetization density: In spin-dynamics, the evolution of discrete spins, i.e. vectors attached to certain (atomic) positions is monitored. Also mapping the *ab initio* results to a model Hamiltonian which contains interactions between spins requires that it is possible to assign a definite spin to an atom, so that it should be possible to write in the vicinity of an atom ν, e.g. within some sphere centered at the nucleus, the magnetization density, $\mathbf{m}(\mathbf{r})$, as

$$\mathbf{m}(\mathbf{r}) = M_\nu \hat{\mathbf{e}}_\nu \tag{35}$$

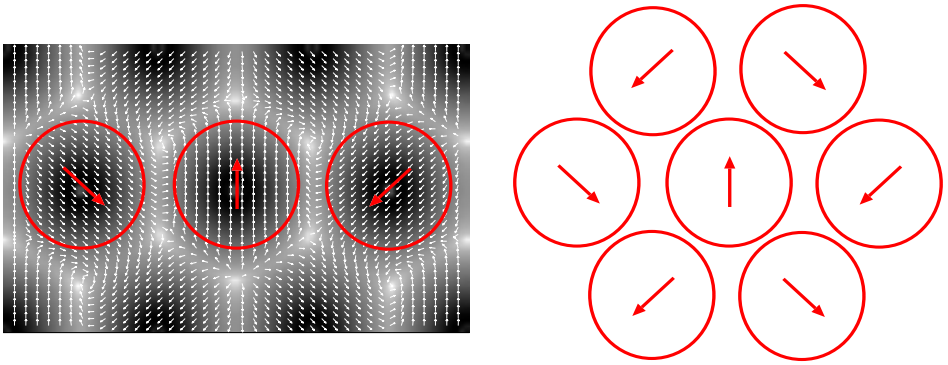

Fig. 13: *Left: ground state magnetization density of a hexagonal Cr monolayer with the Cu(111) in-plane lattice constant; the absolute value of the magnetization is shown in greyscale, the local directions are marked by small arrows. The average magnetization direction around an atom is indicated as red arrows. Right: schematic picture of the magnetic structure (Néel state) of the hexagonal Cr monolayer.*

where M_ν is the magnetization and $\hat{\mathrm{e}}_\nu$ is the magnetization direction. Vector-spin DFT calculations allow to estimate whether Eq. (35) is a good approximation or not (cf. Fig. 13). If the magnetization density in the vicinity of some atom ν is expressible by Eq. (35), then the total energy of a magnetic system as a function of its magnetic structure can be described as a functional $E[\{\hat{\mathrm{e}}_\nu\}]$ of the directions of the magnetic moments at the atoms ν in the magnetic unit cell. In this context collinear states ($\hat{\mathrm{e}}_\nu$ is identical for all atoms) are special solutions where $E[\{\hat{\mathrm{e}}_\nu\}]$ has a local or global maximum or minimum. Therefore, they constitute an important class of magnetic configurations that are often realized in magnetic materials. Unlike in non-spinpolarized DFT it is, however, in practical calculations not guaranteed that the obtained solution, $\mathsf{n}(\mathbf{r})$, is really the ground state and often several metastable solutions can be obtained.

4.1 Ab initio spin-dynamics, magnetic torque

If one is interested in the magnetic ground state of a system of given chemical composition and atomic positions, the final goal is to minimize the functional $E[\{\hat{\mathrm{e}}_\nu\}]$. The dimensionality of this problem will of course depend on the size of the chosen unit cell (some multiple of the chemical unit cell) and this minimization will involve the tricky task to determine the absolute minimum on a high-dimensional total energy surface. In analogy to molecular dynamics, i.e. the problem of minimizing the energy as a function of the atomic positions, we introduce here a spin dynamics, where the magnetic orientations, $\hat{\mathrm{e}}_\nu$, take the role of the variables.
Any vector-spin DFT calculation has to start with a reasonably chosen spin configuration in a prescribed unit cell. On a simple level, one can "relax" the directions of the magnetization at the atoms like a relaxation of the atomic structure (e.g. at a surface) is done. The magnetization directions, $\hat{\mathrm{e}}_\nu$, will then generally change to minimize the total energy (cf. Fig. 14). The final magnetic state, that will be reached, will in general depend on the starting point of the calculation and a more elaborate technique will be needed to avoid being trapped in some local minimum of $E[\{\hat{\mathrm{e}}_\nu\}]$.
To this end we have to develop an equation of motion for the magnetization of an atom. To keep things simple, we will focus on the case, where the magnetization stays collinear within the

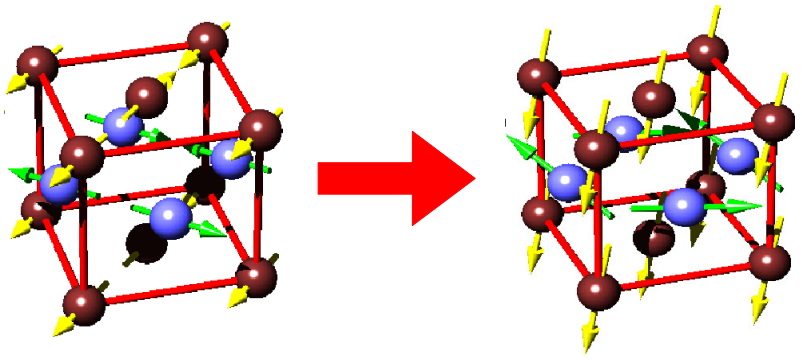

Fig. 14: *Determination of the magnetic ground state of ordered FeMn: the magnetic structure of the disordered alloy is a* $2\mathbf{q}$*-state (left). In an ordered alloy a more complex magnetic arrangement is obtained (right) by "relaxation" of the local spin directions.*

vicinity of the atom. Let us start from the Hamiltonian of Eq. (25) and assume that the external potential matrix, $\mathsf{v}(\mathbf{r})$, has been chosen to be diagonal and the exchange-correlation potential is separated into diagonal and off-diagonal parts. Following Antropov *et al.* [77, 78] we set up a time-dependent analogon of Eq. (25):

$$i\frac{d\Phi}{dt} = \left[H_d - \boldsymbol{\sigma}\cdot\mathbf{B}(\mathbf{r},t)\right]\Phi \quad \text{where} \quad \Phi = \begin{pmatrix} \phi^{(+)} \\ \phi^{(-)} \end{pmatrix}, \tag{36}$$

and H_d is the Hamiltonian that contains now only diagonal parts.
We will now separate the evolution of the magnetization into fast (value of the magnetization) and slow (direction of the magnetization) degrees of freedom. The former part will be described quantum-mechanically, while the latter is treated on a semiclassical level. At a given time, t, the time-independent version of Eq. (36) can be solved for a given magnetization characterized by $\{\hat{\mathbf{e}}_\nu\}$. Now we have to determine an equation of motion for the magnetization $\mathbf{m}(\mathbf{r},t)$.
This equation of motion can be obtained by multiplying Eq. (36) from the left with $\Phi^*\boldsymbol{\sigma}$ and adding the complex conjugate equation. Comparing to the time derivative of Eq. (30) and using the relation $\boldsymbol{\sigma}(\boldsymbol{\sigma}\cdot\mathbf{B}) = \mathbf{B} - i\boldsymbol{\sigma}\times\mathbf{B}$ we get

$$\frac{d\mathbf{m}(\mathbf{r},t)}{dt} = 2\mathbf{m}\times\mathbf{B} + \frac{i}{2}\nabla(\Phi^*\boldsymbol{\sigma}\cdot\nabla\Phi - c.c.). \tag{37}$$

The second term on the right side is complicated and describes longitudinal changes of the magnetization, which we will not consider on this level. Omitting this term, Eq. (37) describes the precession of the magnetization direction at an atom under the influence of the magnetic field generated by the atom itself and other atoms of the crystal.
Returning once more to Eq. (35), we can simplify Eq. (37) and write for the evolution of the magnetization direction in atom ν

$$\frac{d\hat{\mathbf{e}}_\nu}{dt} = -\frac{2}{\mu_\mathrm{B}}\hat{\mathbf{e}}_\nu\times\mathbf{I}_\nu \tag{38}$$

where $\mathbf{I}_\nu = \mu_\mathrm{B}\mathbf{B}$. If we explicitly also want to take into account the effect of other fields acting onto a magnetization direction, e.g. stemming from the spin-orbit interaction (magnetic anisotropy) or dipole-dipole interaction, these fields can be added to Eq. (38) into $\mathbf{I} = \mathbf{I}_\nu + \mathbf{I}_\mathrm{SO} +$

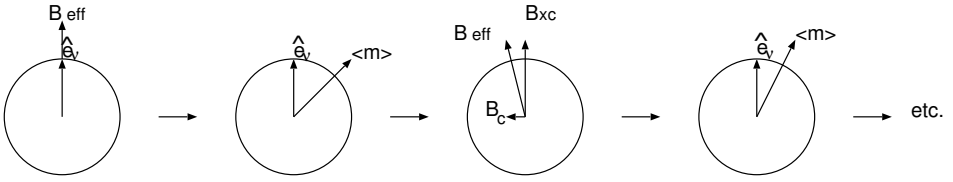

Fig. 15: *Determination of the constraint field: Initially, the effective* $\mathbf{B}$*-field is parallel to the prescribed direction* $\hat{\mathbf{e}}_\nu$ *(left). The resulting magnetization,* $\langle \mathbf{m} \rangle$*, generally is not parallel to this direction. Therefore, a constraint field* $\mathbf{B}_c$ *is introduced, that points in opposite direction to the component of the magnetization that is perpendicular to* $\hat{\mathbf{e}}_\nu$*. Using this* $\mathbf{B}_{\text{eff}}$*, the direction of the magnetization is then adjusted towards* $\hat{\mathbf{e}}_\nu$ *(right).*

$\mathbf{I}_{\mathrm{d-d}}$. More general expressions of Eq. (38), suitable for spin-dynamics with finite temperatures included, can be found in reference [78].
The next question, that has to be answered, is how to determine the fields $\mathbf{I}_\nu$, i.e. given a certain set of magnetization directions $\{\hat{\mathbf{e}}_\nu\}$ what is the torque on a selected magnetic moment [79]. This problem can be solved in constrained vector-spin density functional theory, as introduced in the next section.

4.2 Constrained density functional theory

In general, an arbitrary magnetic configuration given by a set of local (atomic) magnetization directions $\{\hat{\mathbf{e}}_\nu\}$ is not an extremum or a stationary solution of the total energy functional $E\left[\mathsf{n}(\mathbf{r})\right]$. Exceptions are high symmetry states, like collinear magnetic states, a certain class of spin-spiral states (see Sec. 4.4) and particular linear superpositions of several spin-spiral states. The constrained density functional theory developed by Dederichs *et al.* [80] provides the necessary generalization to deal with arbitrary magnetic configurations, i.e. configurations where the orientations of the local moments are constrained to non-equilibrium directions. We define a generalized energy functional $\tilde{E}\left[\mathsf{n}(\mathbf{r})|\{\hat{\mathbf{e}}_\nu\}\right]$, where we ensure that the average magnetization in an atom, $\langle \mathbf{m} \rangle_\nu$, points in the direction $\hat{\mathbf{e}}_\nu$. This condition, $\hat{\mathbf{e}}_\nu \times \langle \mathbf{m} \rangle_\nu = 0$, is introduced by a Lagrange multiplier, $\boldsymbol{\lambda}$, so that [7]

$$\begin{aligned} \tilde{E}\left[\mathsf{n}(\mathbf{r})|\{\hat{\mathbf{e}}_\nu\}\right] &= E\left[\mathsf{n}(\mathbf{r})\right] + \sum_\nu \boldsymbol{\lambda}^\nu \cdot (\hat{\mathbf{e}}_\nu \times \langle \mathbf{m} \rangle_\nu) \\ &= E\left[\mathsf{n}(\mathbf{r})\right] + \mu_B \sum_\nu \mathbf{B}_c^\nu \cdot \langle \mathbf{m} \rangle_\nu . \end{aligned} \tag{39}$$

Here, we recast the Lagrange multiplier in the form of a magnetic field, $\mathbf{B}_c^\nu$, which is the constraining field in atom ν that keeps the local (integrated) magnetic moment, i.e. the magnetization density averaged over the sphere where Eq. (35) holds,

$$\langle \mathbf{m}(\mathbf{r}) \rangle_\nu = \mathbf{M}^\nu = \int_{MT^\nu} \mathbf{m}(\mathbf{r})\, d^3r, \tag{40}$$

parallel to the prescribed direction $\hat{\mathbf{e}}_\nu$.
In an actual constrained local moment (CLM) calculation $\mathsf{n}(\mathbf{r})$ and $\mathbf{B}_c^\nu$ have to be determined self-consistently. The density matrix is calculated in the usual self-consistency cycle. At the

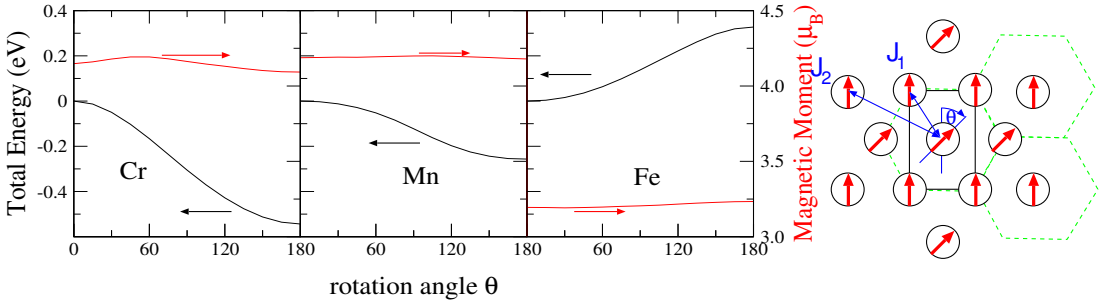

Fig. 16: *Total energy and magnetic moment of hexagonal monolayers of Cr, Mn, and Fe as a function of the angle of the magnetization in a two-atomic unit cell (right). $\theta = 0°$ corresponds to a ferromagnetic state, $\theta = 180°$ is a row-wise antiferromagnetic state. As lattice constant we chose the parameters of the Ag(111) surface. In the schematic picture of the hexagonal monolayer (right) the coupling to nearest neighbors (J_1) and next- nearest neighbors (J_2) is indicated.*

same time, the local constraint fields $\mathbf{B}_c^\nu$ have to be adjusted, until the constraint conditions, $\hat{\mathbf{e}}_\nu \times \langle \mathbf{m} \rangle_\nu = 0$, are fulfilled (cf. Fig. 15). At the end of such a calculation we obtain the self-consistent densities and a set of local constraint $\mathbf{B}$-fields. The total energy of the system is given by the constrained energy functional, Eq. (39).
According to the the Hellmann-Feynman theorem we find that the change of the energy due to a change in magnetization direction, $d\hat{\mathbf{e}}_\nu$, is given by $dE = -\mu_B \mathbf{M}^\nu \cdot (\mathbf{B}_c^\nu \times d\hat{\mathbf{e}}_\nu)$. Therefore, the constraint field can be interpreted as a torque acting on the magnetic moment, in the spirit of the spin dynamics, formulated in the previous section. Thus, we have set up a formalism that allows us to find – at least in principle – the magnetic ground state of a system by spin-dynamics [81]. But CLM calculations can also be used in a different way: In the next section we will describe how they can be used to determine the exchange interactions in a system and utilize these results in models, like the classical Heisenberg model, to obtain information about the ground state, but also about excited states of a magnetic system.

4.3 Mapping onto realistic model Hamiltonians: canted moments

The classical Heisenberg model (2) can be used as a phenomenological starting point for the investigation of the magnetic interaction in a crystal. Although the Heisenberg model was originally introduced for magnetic insulators with localized moments [82], we can also apply Eq. (2) to metallic systems, as shown in Fig. 16. In these hexagonal unsupported monolayers the behavior of the total energy as a function of the relative angle between the atoms can be described as cosine-like function, the exchange coupling constant being negative for Cr and Mn (preferring antiferromagnetic coupling) and positive for Fe (leading to a ferromagnetic ground state). The total energy has been calculated by a constrained DFT calculation as described above. We further see, that the magnetic moment does not change significantly as the spins are rotated, an important requirement for the application of the Heisenberg model.
From the right part of Fig. 16 we can see, that rotating the local magnetic moment direction of one atom in the two-atom unit cell of the hexagonal lattice will change the relative orientation of that atom to four nearest neighbors, but does not affect two of the nearest neighbor (NN) atoms. Likewise, only four of the six second-NN atoms will change the relative orientation to

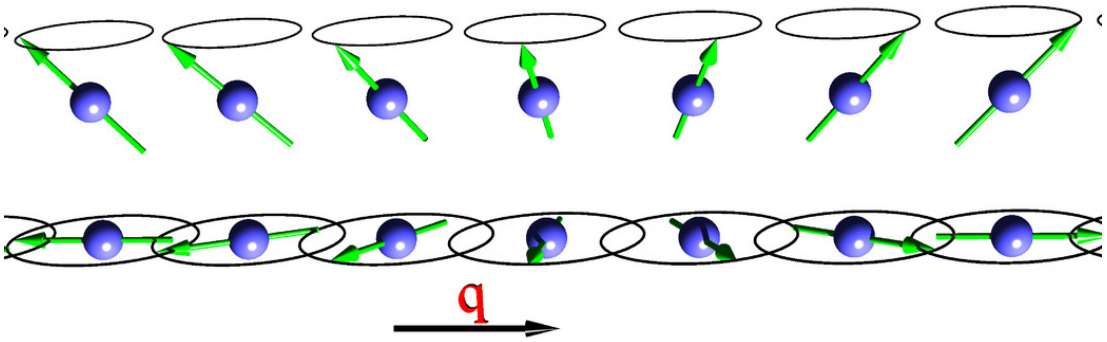

Fig. 17: *Spiral spin-density wave (SSDW) or spin spiral propagating along the with a wavevector* $\mathbf{q}$*. The upper spiral represents a coned-spiral with a cone angle of* $45°$*, the bottom spiral represents a flat spiral, with a cone angle of* $90°$*. Both spirals exhibit a counterclockwise rotational sense expressed by a chirality vector parallel to the* z*-axis.*

the original atom. This leads to an expression for the total energy in the classical Heisenberg model up to second-NN:

$$E = -S^2(J_1 + J_2)(2 + 4\cos\theta) \tag{41}$$

if $\mathbf{S}$ is now the total spin moment treated as a classical vector. This means, from a constrained local moment calculation we can at least estimate the size of $(J_1 + J_2)$. It is not difficult to find other unit cells and rotations that allow the determination of other linear combinations of J_1 and J_2, thereby separating the individual exchange coupling constants [53].
Of course, the energies obtained from the CLM calculation contain contributions of all J_n and also from interactions that are not described by the Heisenberg model. Examples, like the biquadratic interaction or the 4-spin interaction result from hopping processes between four sites, inclusion of spin-orbit interaction gives rise to a third-order process, the so-called Dzyaloshinsky-Moriya interaction [83]. All these different interaction terms can be extracted from a set of suitable *ab initio* calculations (possibly including spin-orbit interaction) and can be used to determine the magnetic ground state within the chosen model.

4.4 Mapping onto realistic model Hamiltonians: spin-spirals

Concluding from the previous section, one way to obtain model parameters like the elements of the above discussed exchange parameters J_{ij} from first principles is to fit the energy expression obtained from the model ansatz to the total energies obtained from electronic structure calculations for different magnetic states. In a periodic crystal it is convenient to replace the quantities in Eq. (2) by their Fourier-transformed equivalents:

$$\mathbf{S}(\mathbf{q}) = \frac{1}{N}\sum_n \mathbf{S}_n e^{-i\mathbf{q}\mathbf{R}_n} \quad \text{and} \quad J(\mathbf{q}) = \sum_n J_{0n} e^{-i\mathbf{q}\mathbf{R}_n}. \tag{42}$$

Exploiting the translational invariance of the lattice, we can then rewrite Eq. (2) as

$$H = -N\sum_{\mathbf{q}} J(\mathbf{q})\mathbf{S}(\mathbf{q})\cdot\mathbf{S}(-\mathbf{q}) \tag{43}$$

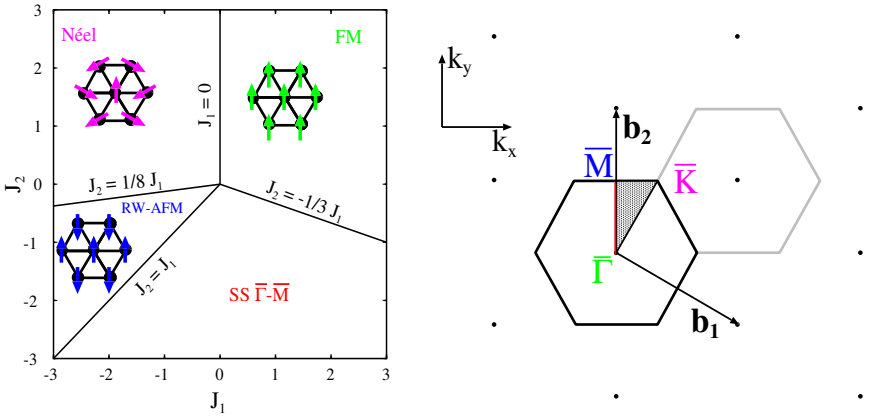

Fig. 18: *Zero temperature phase-diagram of the classical Heisenberg model for the hexagonal lattice in next-nearest neighbor approximation: two collinear, a ferromagnetic (FM) and a row-wise antiferromagnetic (RW-AFM) solution can be obtained, and two non-collinear solutions, the Néel-state and a SSDW with* $\mathbf{q}$*-vectors along the line* $\overline{\Gamma} - \overline{\mathrm{M}}$ *of the Brillouin zone (right). The FM, RW-AFM and Néel-state correspond to SSDWs with* $\mathbf{q}$*-vectors on the high-symmetry points* $\overline{\Gamma}$, $\overline{\mathrm{M}}$ *and* $\overline{\mathrm{K}}$*, respectively.*

where we have to ensure that the length of all spins $\mathbf{S}_n^2 = S^2$ is conserved on all sites n. This condition is fulfilled by solutions of the type [83]

$$\mathbf{S}_n = S\left(\hat{\mathbf{e}}_x \cos(\mathbf{q}\cdot\mathbf{R}_n) + \hat{\mathbf{e}}_y \sin(\mathbf{q}\cdot\mathbf{R}_n)\right) \tag{44}$$

where the unit vectors $\hat{\mathbf{e}}_x$ and $\hat{\mathbf{e}}_y$ just have to be perpendicular to each other, otherwise their directions are arbitrary. Eq. (44) describes a spiral spin-density wave (SSDW) as shown in the lower half of Fig. 17. A more generals form of SSDWs can be obtained, when the magnetization precesses on a cone with an opening angle ϑ:

$$\mathbf{S}_n = S\left(\hat{\mathbf{e}}_x \cos(\mathbf{q}\cdot\mathbf{R}_n)\sin\vartheta + \hat{\mathbf{e}}_y \sin(\mathbf{q}\cdot\mathbf{R}_n)\sin\vartheta + \hat{\mathbf{e}}_z\cos\vartheta\right) \tag{45}$$

as shown in the upper half of Fig. 17.
These SSDWs are general solutions of the classical Heisenberg model for a periodic lattice. From Eq. (43) one can conclude that the SSDW with the lowest total energy will be the one with the propagation vector $\mathbf{Q}$ that maximizes $J(\mathbf{q})$. These will be preferably the high-symmetry points in the Brillouin-zone of $\mathbf{q}$-vectors, and then high-symmetry lines. For example, if $\mathbf{Q} = 0$ maximizes $J(\mathbf{q})$, the solution corresponds to the ferromagnetic state, if $\mathbf{Q} = \hat{\mathbf{e}}_z \frac{\pi}{a_z}$ and a_z is the lattice constant in z-direction, then the structure is layered antiferromagnetic in z-direction. Some other examples – for a hexagonal monolayer – are illustrated in Fig. 18. $T = 0$ many compounds and elemental metals show SSDW ground states. Some examples were shown in Fig. 12.

4.5 Spin-spirals and the generalized Bloch theorem

A very elegant treatment of spin-spirals by first-principle calculations is possible when the generalized Bloch theorem [84, 85, 86] is applied. However, this theorem can only be proved, when spin-orbit coupling is neglected. For this reason the spin-rotation axis will always be considered

as parallel to the z-axis of the spin coordinate-frame. Thus, only the m_x and m_y components are rotated, while m_z does not change. Following Sandratskii [85] we can define a generalized translation, $\mathcal{T}_n$, that combines a lattice translation, $\mathbf{R}_n$, and a spin rotation $\mathbf{U}$ that commutes with the Hamiltonian $\mathcal{H}$. Applying such a generalized translation to $\mathcal{H}\Phi$ yields

$$\begin{aligned} \mathcal{T}_n\mathcal{H}(\mathbf{r})\Phi(\mathbf{r}) &= \mathbf{U}(-\mathbf{q}\mathbf{R}_n)\mathcal{H}(\mathbf{r}+\mathbf{R}_n)\mathbf{U}^\dagger(-\mathbf{q}\mathbf{R}_n)\mathbf{U}(-\mathbf{q}\mathbf{R}_n)\Phi(\mathbf{r}+\mathbf{R}_n) \\ &= H(\mathbf{r})\mathbf{U}(-\mathbf{q}\mathbf{R}_n)\Phi(\mathbf{r}+\mathbf{R}_n) \end{aligned} \tag{46}$$

where $\mathbf{U}(\mathbf{q}\mathbf{R}_n)$ is the spin $1/2$ rotation matrix

$$\mathbf{U}(\mathbf{q}\mathbf{R}_n) = \begin{pmatrix} e^{-i\varphi/2} & 0 \\ 0 & e^{i\varphi/2} \end{pmatrix}, \quad \varphi = \mathbf{q}\cdot\mathbf{R}_n. \tag{47}$$

In analogy with the proof of Bloch's theorem [87] it follows that the eigenstates can be chosen such that

$$\mathcal{T}_n\Phi(\mathbf{k},\mathbf{r}) = \mathbf{U}(-\mathbf{q}\mathbf{R}_n)\Phi(\mathbf{k},\mathbf{r}+\mathbf{R}_n) = e^{i\mathbf{k}\cdot\mathbf{R}_n}\Phi(\mathbf{k},\mathbf{r}). \tag{48}$$

Since these eigenstates are labeled with the same Bloch vector $\mathbf{k}$ as the eigenstates of the translation operator without the spin rotation, the lattice periodic part of these states follows the chemical lattice, $\mathbf{R}_n$, i.e. we can calculate the spin spiral state in the chemical unit cell and $\mathbf{k}$ denotes a $\mathbf{k}$-vector of the reciprocal chemical lattice. The resulting eigenstates of the Hamiltonian $\mathcal{H}$ have the form

$$\psi_{\mathbf{k},\nu}(\mathbf{r}) = \begin{pmatrix} \psi^{(\uparrow)}_{\mathbf{k},\nu}(\mathbf{r}) \\ \psi^{(\downarrow)}_{\mathbf{k},\nu}(\mathbf{r}) \end{pmatrix} = \exp(i\,\mathbf{k}\cdot\mathbf{r}) \begin{pmatrix} \exp(-i\,\frac{1}{2}\,\mathbf{q}\cdot\mathbf{r})\; u^{(\uparrow)}_{\mathbf{k},\nu}(\mathbf{r}) \\ \exp(+i\,\frac{1}{2}\,\mathbf{q}\cdot\mathbf{r})\; u^{(\downarrow)}_{\mathbf{k},\nu}(\mathbf{r}) \end{pmatrix} \tag{49}$$

with the $\mathbf{q}$-vector of length $|q|$ pointing along the propagation direction of the spiral and the functions $u^{(\uparrow)}_{\mathbf{k},\nu}(\mathbf{r})$, $u^{(\downarrow)}_{\mathbf{k},\nu}(\mathbf{r})$ possessing the period of the chemical lattice.
In a reciprocal-space method, i.e. when all quantities like potential or wavefunctions are expressed as Fourier-transforms, the computational effort scales with the size of the unit cell. Without the application of the generalized Bloch theorem the investigation of spin spiral states requires very large unit cells, and a description of SSDWs that are incommensurate with the lattice would be not possible.
Since the spin-spiral is the exact solution of the classical Heisenberg model at T$=0$, it is believed that they cover a large and important part of the phase space of possible spin states. Thus among all possible magnetic states, spin-spirals are the next relevant class of spin states besides the high-symmetry magnetic states, i.e. the ferromagnetic, antiferromagnetic, or ferrimagnetic configurations.
A further computational simplification can be reached, when the SSDW is considered just as a small perturbation to the parent (most often ferromagnetic) structure. This may be justified in the limit of small $\mathbf{q}$-vectors or small opening angles ϑ (cf. Eq. (45)). The limit of $\vartheta \to 0$ is particularly important in the study of finite temperature effects, since it describes elementary perturbations of the collinear ground state. In this limit again the magnetic force theorem [76] can be applied, thus reducing the computational efforts significantly [88].
In real-space methods the calculation of $J(\mathbf{q})$ is most conveniently done via the right of Eq. (42), i.e. the evaluation of J_{0n}. In this case the direction of the magnetization at a reference atom, 0, is perturbed and the response on the other atoms, n, calculated. Also in this case a kind of magnetic force theorem can be used [64].

4.6 Calculating the DM interaction with periodic spin spirals

In order to determine the DM-strength $\mathbf{D}$ from first principles we follow the same strategy as above and fit an appropriate energy expression obtained from the model ansatz to the total energies obtained from electronic structure calculations for different magnetic states. We start with the model ansatz (18) and assume a situation where the system is in a collinear magnetic state without DM-interaction, the DM-interaction is much smaller than the exchange ($D << J$) and thus the DM-interaction can only introduce long-period spirals. Under this assumption we can go from a discrete model (18) to a micromagnetic model that is continuous in space coordinates. We assume further that the easy axis is out-of-plane $\mathbf{K} = (0, 0, K)$ and the the hard axis is oriented parallel to $\mathbf{D} = (0, D, 0)$, then the anisotropy term also favors a magnetization that is confined to the plane normal to $\mathbf{D}$. In such a system with $\mathbf{m} \perp \mathbf{D}$, we can describe the magnetization as a planar spiral with only one angle φ ($\mathbf{m} = \hat{\mathbf{e}}_x \cos\varphi + \hat{\mathbf{e}}_z \sin\varphi$). For homogeneous spin spirals (i.e. spirals with $\dot{\varphi}(x) = q = \text{const}$ or a constant canting angle $\arccos(\mathbf{S}_i \cdot \mathbf{S}_{i+1})$ between the magnetizations of two adjacent lattice sites) the magnetic structure has a period of $\lambda_{\text{hs}} = 2\,\pi/q$ and the energy density E/λ_{hs} of the micromagnetic model becomes

$$\frac{q}{2\,\pi}\,E(q) = \frac{q}{2\,\pi}\int_0^{\frac{2\,\pi}{q}} \mathrm{d}x\,\left(\,A\,q^2 + D\,q + K\sin^2(q\,x)\,\right) = A\,q^2 + D\,q + \tfrac{1}{2}\,K\;. \tag{50}$$

Thus, we can obtain our model parameters A for the exchange and D from a quadratic and a linear fit to the dispersion curve $q\,E(q)$, with latter obtained from first-principles calculations. In order to determine the anisotropy constant K, we can perform independent calculations of collinear configurations with $\varphi = 0$ and $\varphi = \pi$.

Since the micromagnetic model is valid in the limit of slow spatial rotations, relation (50) holds only for homogeneous spin spirals with large period lengths. This presents a formidable problem, since the size of the unit cell that one can treat is limited by the computing facilities. The generalized Bloch theorem [84, 85, 86] cannot be applied here directly due to the presence of the spin-orbit interaction. We employ a perturbative scheme in order to deal with these large magnetic superstructures: We calculate the rotations self-consistently on the basis of the Hamiltonian $\mathcal{H}_0$, but treat the spin-orbit coupling as a perturbation. Thereby, we make use of the local force theorem [89, 90]. If we neglect spin-orbit coupling, the orientation of the magnetic moments with respect to the crystal lattice is irrelevant and we can calculate the electronic structure of a homogeneous spin spiral within the chemical unit cell by applying a generalized Bloch theorem [84, 85, 86].

In a next step, we apply the spin-orbit coupling operator $\mathcal{H}_{\text{so}}$ in second variation, i.e. we expand the eigenfunctions of $\mathcal{H}_0 + \mathcal{H}_{\text{so}}$ in eigenfunctions of $\mathcal{H}_0$ and construct the Hamiltonian matrix with the matrix elements $\langle\psi_{\mathbf{k}',\nu'}|\mathcal{H}_0 + \mathcal{H}_{\text{so}}|\psi_{\mathbf{k},\nu}\rangle$. Since we can neglect all states of high energy, this procedure reduces the size of the Hamiltonian matrix drastically. The spin-orbit coupling is well described by

$$\mathcal{H}_{\text{so}} = \sum_\alpha \frac{1}{r_\alpha}\frac{\mathrm{d}V_\alpha(r_\alpha)}{\mathrm{d}r_\alpha}\,\boldsymbol{\sigma}\cdot\hat{\mathbf{L}}_\alpha = \begin{pmatrix} \mathcal{H}_{\text{so}}^{(\uparrow,\uparrow)} & \mathcal{H}_{\text{so}}^{(\uparrow,\downarrow)} \\ \mathcal{H}_{\text{so}}^{(\downarrow,\uparrow)} & \mathcal{H}_{\text{so}}^{(\downarrow,\downarrow)} \end{pmatrix}\,, \tag{51}$$

where the index α denotes the atoms. Since only the spin-independent part of the potential enters $\mathcal{H}_{\text{so}}$, its real-space representation possesses the period of the chemical lattice. This allows

us to write the matrix elements in the form

$$\begin{aligned}
\langle\psi^{(\uparrow)}_{\mathbf{k}',\nu'}|\,\mathcal{H}^{(\uparrow,\uparrow)}_{\mathrm{so}}\,|\psi^{(\uparrow)}_{\mathbf{k},\nu}\rangle &= \int\mathrm{d}\mathbf{r}\ \mathrm{e}^{i\,(\mathbf{k}-\mathbf{k}')\cdot\mathbf{r}}\quad u^{(\uparrow,\uparrow)}(\mathbf{r})\ ,\\
\langle\psi^{(\uparrow)}_{\mathbf{k}',\nu'}|\,\mathcal{H}^{(\uparrow,\downarrow)}_{\mathrm{so}}\,|\psi^{(\downarrow)}_{\mathbf{k},\nu}\rangle &= \int\mathrm{d}\mathbf{r}\ \mathrm{e}^{i\,(\mathbf{k}-\mathbf{k}'+\mathbf{q})\cdot\mathbf{r}}\ u^{(\uparrow,\downarrow)}(\mathbf{r})\ ,\\
\langle\psi^{(\downarrow)}_{\mathbf{k}',\nu'}|\,\mathcal{H}^{(\downarrow,\uparrow)}_{\mathrm{so}}\,|\psi^{(\uparrow)}_{\mathbf{k},\nu}\rangle &= \int\mathrm{d}\mathbf{r}\ \mathrm{e}^{i\,(\mathbf{k}-\mathbf{k}'-\mathbf{q})\cdot\mathbf{r}}\ u^{(\downarrow,\uparrow)}(\mathbf{r})\ ,\\
\langle\psi^{(\downarrow)}_{\mathbf{k}',\nu'}|\,\mathcal{H}^{(\downarrow,\downarrow)}_{\mathrm{so}}\,|\psi^{(\downarrow)}_{\mathbf{k},\nu}\rangle &= \int\mathrm{d}\mathbf{r}\ \mathrm{e}^{i\,(\mathbf{k}-\mathbf{k}')\cdot\mathbf{r}}\quad u^{(\downarrow,\downarrow)}(\mathbf{r})
\end{aligned} \tag{52}$$

with lattice-periodic functions $u^{(\uparrow,\uparrow)}$, $u^{(\uparrow,\downarrow)}$, $u^{(\downarrow,\uparrow)}$, $u^{(\downarrow,\downarrow)}$. Obviously, these matrix elements are non-zero if and only if the exponents are zero. If we choose a $\mathbf{q}$-vector that is commensurate with the reciprocal lattice (i.e. a spiral that is commensurate within a certain supercell) and a $\mathbf{k}$-grid that is commensurate to the $\mathbf{q}$-vector, then we obtain a block-diagonal and sparse Hamiltonian matrix. Each block contains the matrix elements from all $\mathbf{k}$-vectors that are connected by $\mathbf{q}$ (cf. Fig. 19). Note, that $\mathbf{q}$ is a reciprocal lattice vector of the large magnetic unit cell in which the spin spiral is commensurate.
For large systems, the Hamiltonian matrix that is shown in Fig. 19 is too large for straightforward diagonalization. But since we are applying the local force theorem, we only need to know the sum of occupied eigenvalues. This allows to use a perturbative technique that requires exact diagonalization only in a subspace close to the Fermi energy and exploits the sparseness [91].

5 Beyond the ground state

5.1 Low temperatures: magnons and spin waves

SSDWs are sometimes also called frozen magnons, since a spin-spiral looks like a "snap shot" of a single magnon at a fixed time. Spin-spiral calculations can therefore be used to simulate

$$H_{\{\mathbf{k}\}} = \Big(\ \delta_{\mathbf{k},\mathbf{k}'}\delta_{\nu,\nu'}\,\epsilon_{\mathbf{k},\nu} + \langle\psi_{\mathbf{k},\nu'}|\mathcal{H}_{\mathrm{so}}|\psi_{\mathbf{k},\nu}\rangle\ \Big)_{\substack{\mathbf{k},\mathbf{k}'\\ \nu,\nu'}} =$$

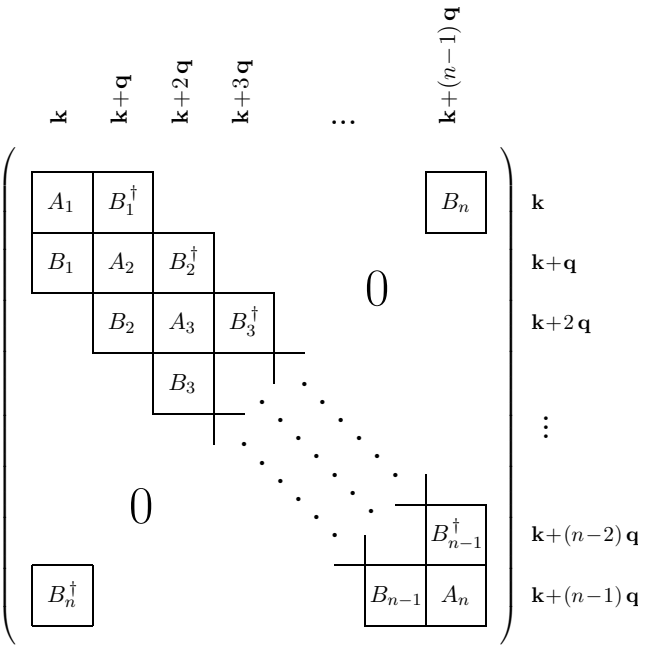

Fig. 19: *Block of the Hamiltonian matrix for spin-spiral basis functions.*

the effect of temperature on a magnetic system in the adiabatic approximation, in particular at very low temperatures, when magnons with long wavelength dominate.
At low, but finite temperatures, collective spin-wave excitations or magnons are excited in the ferromagnetic crystal. These magnons can again be characterized by their wave-vector $\mathbf{q}$. In the long wavelength limit, i.e. around $\mathbf{q} = 0$ the spin-wave dispersion behaves almost quadratically and can be described as Dq^2. The spin stiffness, D, characterizes the magnetic properties of a ferromagnet at low temperatures and can also be calculated from the exchange coupling constants:

$$D = \frac{2}{3M} \sum_n J_{0n} R_{0n}^2. \tag{53}$$

Here, M is the magnetic moment of the ferromagnetic state. Some results of *ab initio* calculations are given in Table 2. For Fe and Co agreement with experimental data is reasonable, but

Table 2: *Calculated and experimental spin-wave stiffness (D) for Fe, Co and Ni. The theoretical data were obtained in different approximations as described by Rosengaard and Johansson [92] [th.(1)], Shallcross and coworkers [67] [th.(2)] and Pajda et al. [93] [th.(3)], experimental data was taken as cited in these references.*

	D (meV Å^2)			
	th.(1)	th.(2)	th.(3)	exp.
Fe (bcc)	247	322, 313	250	280, 314, 330
Co (fcc)	502	480, 520	663	510, 580
Ni (fcc)	739	541, 1796	756	422, 550, 555

for Ni most methods fail to reproduce the experimental spin stiffness.

5.2 High temperatures: $T_{\rm C}$ and $T_{\rm N}$

Let us now see, how higher temperatures will influence the magnetic order in a ferromagnetic solid. Staying within the Heisenberg model, we will assume that the magnitude of the magnetic moments at the atoms will – in first approximation – not be changed, and discuss just their mutual orientation. At $T = 0$ the spin at a selected atom will be fixed in parallel direction to the spins at all other atoms by an effective field that will be proportional to $S\sum_n J_{0n} = SJ_0$. At a finite temperature T, this field, that acts on the spin at site 0 is reduced due to the thermal fluctuation on the sites n. The thermal average of the projection of the spin at site n on the spin at site 0 is denoted as $\langle S(\mathbf{R}_n)\rangle$. In the "mean field approximation" (MFA), it is assumed that the effective field at finite temperatures that acts on spin 0 is:

$$B_{\rm eff} = \sum_n J_{0n} \langle S(\mathbf{R}_n)\rangle \tag{54}$$

In this model it is possible to calculate the temperature-dependence of the average magnetization of the solid and, specifically, the temperature where the average magnetization vanishes, the critical temperature. For a ferromagnet this temperature is called Curie temperature and in the MFA it is given by

$$T_{\rm C} = \frac{2S(S+1)}{3k_{\rm B}} J_0 \tag{55}$$

It has to be mentioned, that in most cases the MFA severely overestimates $T_{\rm C}$ (by about 20 to 50%, depending on the lattice). Nevertheless, it gives a simple estimate of the ordering temperature in systems, where the approximations of the Heisenberg model are reasonable. On the other hand, some properties, like the – material independent – critical exponents, are in any case not usefully reproduced by the MFA.
On a more sophisticated level, the "random phase approximation" (RPA) can give quite reliable results. In contrast to the MFA, where the thermal averaging was done over the sites n that determine $B_{\rm eff}$, here the Hamiltonian is first transformed into reciprocal space (Eq. (43)), and then the averaging is done over one of the Fourier components:

$$H = -N \sum_{\mathbf{q}} J(\mathbf{q}) \mathbf{S}(\mathbf{q}) \cdot \langle \mathbf{S}(-\mathbf{q}) \rangle \tag{56}$$

If the term $S(S+1)$ is included in the exchange coupling constants (as it is usually done, when the J's are determined from first-principles calculations), then the Curie temperature in the MFA and RPA can be expressed as

$$k_{\rm B} T_{\rm C}^{\rm MFA} = \frac{2}{3} J_0 \qquad k_{\rm B} T_{\rm C}^{\rm RPA} = \frac{2}{3} \left(\sum_{\mathbf{q}} \frac{1}{J(\mathbf{q})} \right)^{-1} \tag{57}$$

From these expressions it is obvious, that calculating $T_{\rm C}$ in the RPA involves not more information that what is needed on a mean-field level, if the exchange coupling constants are calculated in reciprocal space by using the generalized Bloch theorem.
Also for antiferromagnets (or, generally spin-spiral states characterized by a vector $\mathbf{Q}$) expressions for the ordering temperature, the Néel temperature $T_{\rm N}$, can be derived. In the MFA with $S(S+1)$ again included in J, this is given simply by

$$k_{\rm B} T_{\rm N}^{\rm MFA} = \frac{2}{3} J(\mathbf{Q}) \,, \tag{58}$$

while a slightly more involved expression can be derived in the random phase approximation [64]. Comparison of these results with experimental values gave reasonable results, e.g. for bcc europium Néel temperatures of 147 K and 110 K were obtained in MFA and RPA, respectively [64]. These values have to be compared to the experimental $T_{\rm N}$ of 90.5 ± 0.5 K.
Although there exist several more methods to calculate critical temperatures from DFT results, we will outline here just one further possibility, which seems to be rather flexible and appropriate for many systems with different magnetic ground states: the Monte Carlo technique (MC) allows to study finite-temperature magnetic properties by implementation of a Heisenberg Hamiltonian (Eq. (2), possible with extensions like biquadratic terms or an uniaxial anisotropy (see below)), into a Metropolis algorithm [94]. Unit cells of different size are then studied so that finite-size effects can be eliminated. In these unit cells the evolution of the magnetic property in question (in our case the average magnetization) as a function of temperature can then be monitored. The method will be discussed in detail in Lecture C1 *Magnetic phase transitions: from density functional theory to Monte Carlo simulations.*
Results of *ab initio* calculations of the Curie temperature of Fe, Co and Ni are presented in Table 3. From this table one can easily see that, compared to RPA, the MFA typically overestimates $T_{\rm C}$ by 25–50%. For Fe and Co RPA gives quite good estimates of the Curie temperature, while for Ni $T_{\rm C}$ is underestimated in both approximations. MC simulations work better for Ni and Fe, but give a too low $T_{\rm C}$ for Co.

Table 3: *Calculated and experimental Curie temperature $T_{\rm C}$ for some ferromagnetic materials. MFA and RPA data for Fe, Co and Ni taken from Pajda et al. [93], MFA2 results and experimental values as quoted by Shallcross and coworkers [67], while the MC results were obtained by Rosengaard and Johansson [92]. Data for Gd can be found in the papers of Kurz et al. [68] and Turek and coworkers [95].*

	$T_{\rm C}$ (K)				
	MFA	MFA2	RPA	MC	exp.
Fe (bcc)	1414	$550, 1190$	950	1060	$1044-1045$
Co (fcc)	1645	$1120, 1350$	1311	1080	$1388-1390$
Ni (fcc)	397	$320, 820$	350	510	$624-631$
Gd (hcp)	334				293

While we quoted here results for "simple" metals, it is nowadays possible to investigate in the same manner the temperature dependent properties of complex multicomponent systems, e.g. half-metallic Heusler alloys [96] or dilute magnetic semiconductors [97]. In this way, materials for modern spintronic applications can be studied at physically relevant temperatures and their detailed magnetic properties can be predicted on the basis of quantum-mechanics. The combination of advanced numerical techniques and massively parallel supercomputers makes computational material science one of the most rapidly growing fields of physics with relevance for basic and applied science.

6 Examples: Low-dimensional magnets at surfaces

6.1 Non-collinear configurations of $3d$-impurities on ferromagnetic surfaces

In this section we provide some examples [98, 99, 100, 101] for non-collinear configurations of $3d$-dimers and multimers on the surfaces of ferromagnets. Here, the unperturbed surfaces are ferromagnetic with a collinear moment configuration. Thus, the Green function G^0 and t-matrix, $t^0 = \int dr j_l(r) V(r) R_l(r)$, where V is the potential of the atom, j the Bessel function and R the regular solution of the Schrödinger equation, of the ideal surface are diagonal in spin-space

$$G^0(E) = \left\{ \begin{array}{cc} G^0_{\uparrow\uparrow}(E) & 0 \\ 0 & G^0_{\downarrow\downarrow}(E) \end{array} \right\}, \quad t^0(E) = \left\{ \begin{array}{cc} t^0_{\uparrow\uparrow} & 0 \\ 0 & t^0_{\downarrow\downarrow} \end{array} \right\}, \tag{59}$$

while non-collinear states lead to non-diagonal t-matrices for the impurity atoms and the surrounding substrate neighbors

$$t(E) = \left\{ \begin{array}{cc} t_{\uparrow\uparrow} & t_{\uparrow\downarrow} \\ t_{\downarrow\uparrow} & t_{\downarrow\downarrow} \end{array} \right\}. \tag{60}$$

The basic approximation with respect to non-collinearity consists of the assumption, that the exchange-correlation potential of each atom $\mathbf{R}^n$ has a unique quantisation axis $\mathbf{e}^n$, being common to the whole cell n and determined by the direction of the local moment $\mathbf{M}^n$ in cell n. In this local reference frame, the t-matrix t^n is diagonal

$$t^n_{loc} = \left\{ \begin{array}{cc} t^n_{\uparrow\uparrow} & 0 \\ 0 & t^n_{\downarrow\downarrow} \end{array} \right\} \tag{61}$$

and the local radial functions R^n_ℓ and H^n_ℓ are spin-dependent as in a collinear calculation. However, the Dyson equation describing the multiple scattering events has to be evaluated in a common global frame of reference, as e.g. determined by the magnetisation direction of the substrate. The corresponding transformed t^n-matrices are given by

$$t^n_{glob}(E) = U_n \, t^n_{loc}(E) \, U^t_n \tag{62}$$

where the rotation matrix U_n in spin space is given by

$$U_n = \left(\begin{array}{cc} \cos(\frac{\theta_n}{2}) \, e^{-i\phi_n/2} & -\sin(\frac{\theta_n}{2}) \, e^{-i\phi_n/2} \\ \sin(\frac{\theta_n}{2}) \, e^{i\phi_n/2} & \cos(\frac{\theta_n}{2}) \, e^{i\phi_n/2} \end{array} \right) \tag{63}$$

Here θ_n and ϕ_n are the polar angles defining the direction of the local moment $\mathbf{M}^n$ with respect to the substrate moments.

The basic reason for non-collinear states is "frustration", arising from the competition between ferromagnetic and antiferromagnetic coupling. In addition, also spin-orbit coupling can lead to a non-alignment of the local moments. However, this is a very weak effect for transition metals, for which frustration is much more important. We will illustrate this in the following for transition-metal dimers on the Ni(001) surface.

Let us start with single $3d$ adsorbate atoms on Ni(001). The calculations show, that the $3d$ adatoms have large and stable local moments. The moments of the Co, Fe and Mn adatoms couple ferromagnetically to the substrate moments, while the V and Cr moments prefer an antiferromagnetic coupling to the substrate. The situation of two $3d$-adatoms forming a dimer is illustrated in Fig. 20. Three kinds of dimers are shown: Dimer 1 with the adatoms on nearest neighbor sites, Dimer 2 with the adatoms on second neighbor sites and Dimer 3 on fourth neighbor site. For the Dimer 2 and dimers with larger separation the interaction of the dimer atoms is very small and the configuration is dominated by the interaction with the substrate, meaning that these dimers show the same behavior as the single adatoms, coupling antiferromagnetically to the substrate in the case of V and Cr and ferromagnetically in the case of Mn and Fe, such that both adatoms are parallel aligned to each other. The same is also correct for the NN dimers of Fe or V, where the dimer atom interaction is strongly ferromagnetic (for Fe) or weakly antiferromagnetic (for V). In the case of the Cr and Mn dimers the situation is more complicated, since the interaction of the dimer atoms is strongly antiferromagnetic, favouring an antiferromagnetic pairing of the two moments. However, this is in contradiction to the interaction with the substrate moments, which as explained above, favours a parallel alignment of the impurity moments. Therefore frustration occurs, which can lead to a non-collinear ground state.

The situation is most easily explained, if a model operator in form of the classical Heisenberg model (2) applied to the interaction of the two adatoms $A = 1, 2$ and their interaction with the Ni moments, which for simplicity are assumed to be fixed, the Hamiltonian is

$$H = -J_{A-A} \cos(\theta_1 - \theta_2) - 4J_{A-Ni}(\cos\theta_1 + \cos\theta_2) \tag{64}$$

where θ_1 and θ_2 are the angles with the respect to the substrate magnetisation.

Let us now consider two typical spin configurations, shown in Fig. 21(a) and Fig. 21(b). Fig. 21(a) refers to a collinear configuration, which we call ferrimagnetic, since the two moments, being

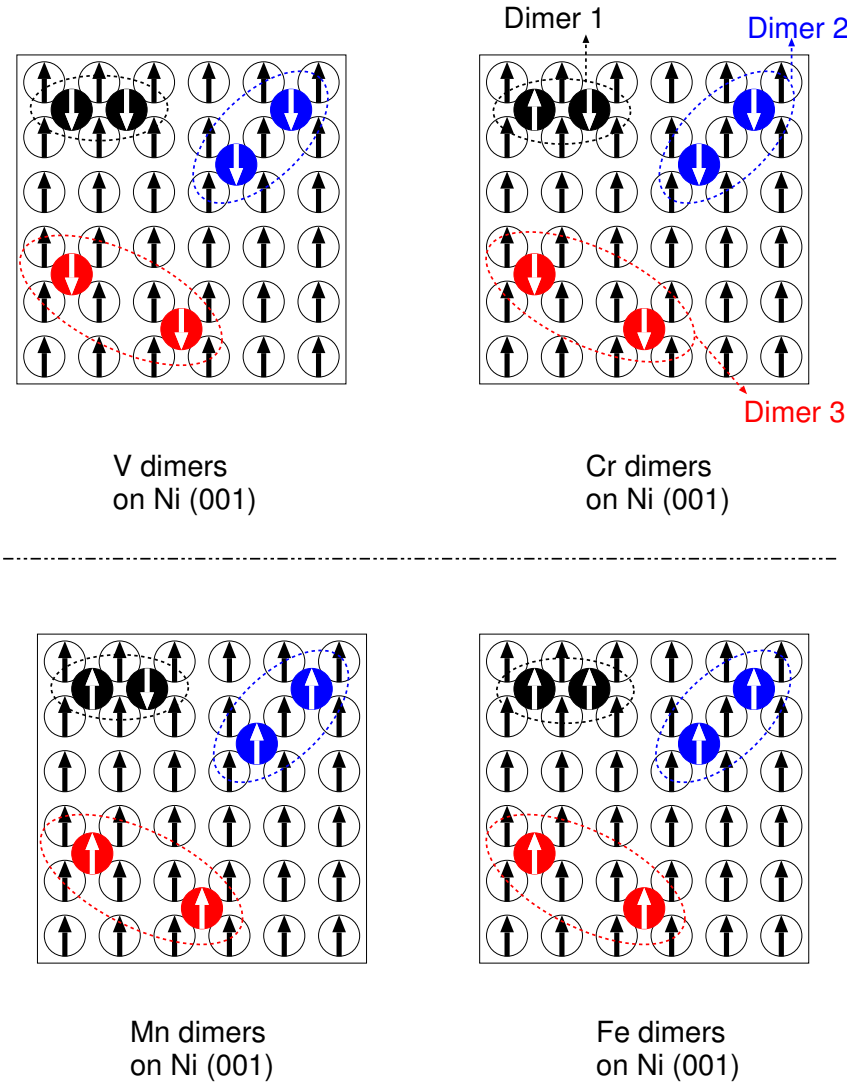

Fig. 20: *Different geometrical configurations considered for dimers at the surface of Ni(001). Dimer-1–type corresponds to the case where the atoms are first neighboring atoms, dimer-2–type where the atoms are second NN and finally dimer-3–type to fourth NN. The collinear magnetic ground state are also shown for V, Cr, Mn and Fe dimers.*

antiferromagnetically aligned, are not equivalent anymore, resulting in a small, but finite total moment. This configuration is also a selfconsistent solution of the Kohn-Sham equations, if the collinear constraint is removed. This can be understood for example from the Heisenberg model Eq. (64), since $\theta_1 = 0, \theta_2 = 180^o$ and small variations around these angles change the cos-values in Eq. (64) only in second order, so that the total energy is an extremum. The configuration in Fig.21(b) is noncollinear, but has the same energy as the collinear configuration (a), since in configuration (a) the interaction of the two adatoms with the substrate atoms cancel each other, while in configuration 21(b) they vanish for both atoms since $\cos\theta_1 = 0 = \cos\theta_2$. However this configuration is not a selfconsistent solution of the non-collinear Kohn-Sham equations, since a small variation $\Delta\theta_1$ and $\Delta\theta_2$ around the values of 90^o, respectively 270^o, changes the energy linearly in $\Delta\theta_1$ and $\Delta\theta_2$. Thus there exists a force which tilts the moments slightly towards or

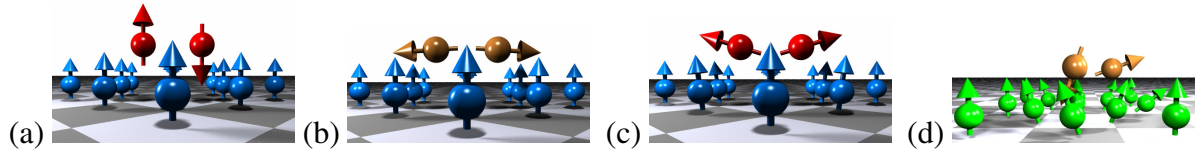

(e)

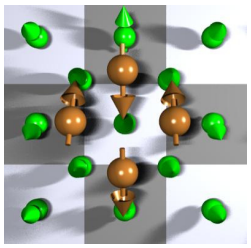

Fig. 21. *Most stable configurations of Cr and Mn dimer on Ni (in blue) obtained with (a) the collinear and (b)-(c) the non-collinear KKR method [98]. For Cr(Mn) the rotation angle with respect to the z axis is equal to 94.2°(72.6°) and the collinear(non-collinear) state is the ground state (see text). (d) shows a side view of the stable Cr trimer on the fcc Fe(001) surface (in green), with two Cr atoms pointing down (the second one cannot be seen), one Cr atom pointing up. (e) shows the stable Cr tetramer on the same fcc Fe surface.*

away from the surface, depending on the sign of J_{A-Ni}. In fact the configuration (b) is the non-collinear solution for a Cr-dimer. With a rotation angle of 94^o, deviating only slightly from 90^o (which can hardly be seen in the figure), a small energy is gained due to the antiferromagnetic coupling with the substrate $(J_{Cr-Ni} < 0)$. In contrast to this the configuration in Fig. 21(c) is the selfconsistent solution for a Mn-dimer, which prefers a ferromagnetic coupling with the substrate atoms ($J_{Mn-Ni} > 0$). Here the angle with respect to the z-axis is 73^o, the deviation from 90 % is much larger. The *ab initio* calculation shows, that this is the ground state for the Mn-dimer. However for the Cr-dimer the collinear solution of Fig. 21(a) is the ground state, which is in contradiction to the Heisenberg model and arises from small changes of the local moments upon rotation, an effect which cannot be described by this model.
In Fig. 21(d) and (e) we show two other non-collinear configurations obtained in the *ab initio* calculations, the configurations for compact Cr-trimers and Cr tetramers on fcc Fe_{3ML}/Cu(001). The exchange interactions are in this case very similar, except that the antiferromagnetic coupling of the Cr-adatoms to the Fe substrate atoms is considerably stronger. In both cases the Cr-Cr interaction is strongly antiferromagnetic. For the trimer, it is most important, that the effective interaction with the substrate moments is non-zero in the collinear configuration, but zero in the planar configuration. Thus the (basically) collinear configuration with the outer Cr-atoms antiferromagnetically aligned to the surface moments and the central Cr atom ferromagnetically aligned is favoured. However an additional small tilting occurs, in particular for the wrongly aligned central Cr atom, which further lowers the energy, so that also this configuration becomes non-collinear.
For the tetramer, the neighboring Cr-atoms couple again antiferromagnetically. For the in-plane configuration, similar to the dimer, the effective interaction with the substrate moments vanishes, however slight tiltings of the moments towards the surface lead to an additional energy gain stabilising the in-plane configuration.

6.2 Monolayers with complex spin structures

Antiferromagnetic interactions on a triangular lattice are the origin of frustrated spin systems. In recent years the epitaxial growth of such ultra-thin films has been studied intensively by various experimental techniques. In particular, pseudo-hexagonal c(8×2)Mn films on Cu(100) [102], Mn films on the (111) surfaces of fcc Pd [103], Ir [104], Cu [105, 106, 107], and MgO [108] and on the (0001) surface of Ru [109] and Co [110] have been prepared and analyzed. But also

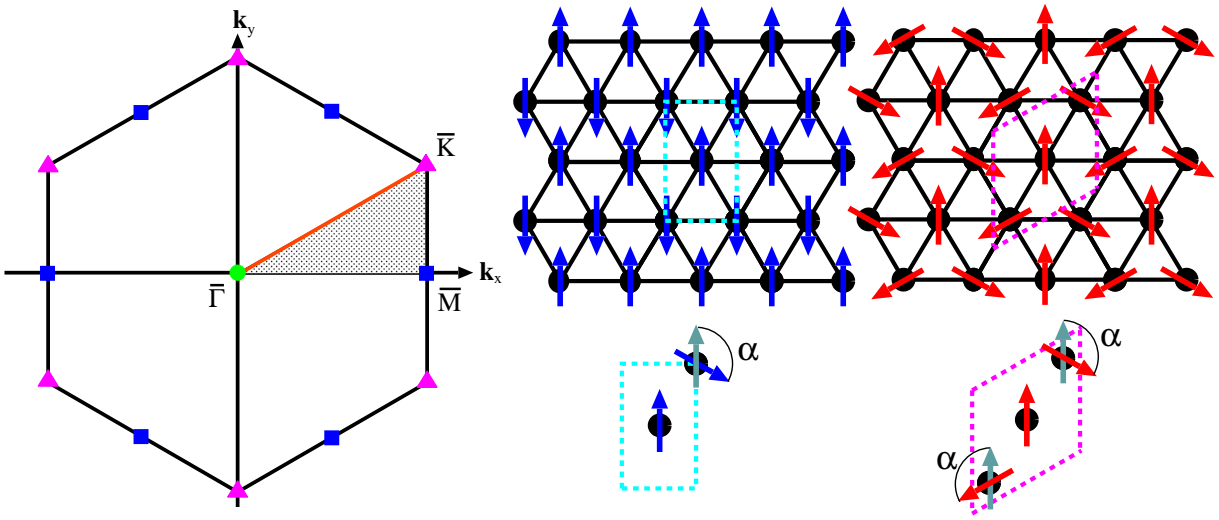

Fig. 22: *(Left:) The hexagon shows the first BZ of the 2D hexagonal Bravais lattice. The gray-shaded area indicates the irreducible part. (Center:) The RW-AFM structure. (Right:) the coplanar non-collinear Néel* ($120°$) *structure. Indicated are the corresponding two- and three-atom unit cells and the continous paths, which connect the corresponding magnetic structure to the FM state.*

other ultra-thin hexagonal films, e.g. Cr and V on Pt(111) and Ru(0001) [111, 112, 113], have been investigated.

To obtain an overview of all relevant spin-structures we develop first a zero-temperature phase diagram in the context of the Heisenberg model. As discussed in Section 2.1 the magnetic ground states are SSDWs, most likely with a commensurate propagation vector $\mathbf{q}_{\|}$ located at the high-symmetry points in the first 2DBZ of a 2D Bravais lattice. For the 2DBZ of the triangular (hexagonal) lattice, displayed in Fig. 22 (Left), the high-symmetry points are the corner points $\overline{\Gamma}$, $\overline{\mathrm{K}}$, and $\overline{\mathrm{M}}$ of the irreducible wedge of the 2DBZ (I2DBZ). The $\overline{\Gamma}$-point corresponds to the ferromagnetic solution. The $\overline{\mathrm{K}}$-point corresponds to a $120°$ Néel state (Fig. 22 (Center)), a 2D coplanar spin structure with three atoms in a $(\sqrt{3} \times \sqrt{3})$ R$30°$ unit cell for which the relative angle between the spins at the different sites is always $120°$. The $\overline{\mathrm{M}}$-point corresponds to row-wise antiferromagnetic (RW-AFM) configuration (Fig. 22 (Right)), which can be described by a rectangular unit cell with two antiferromagnetically aligned atoms. Magnetic ground states with incommensurate $\mathbf{q}_{\|}$-vectors are also possible preferentially with $\mathbf{q}_{\|}$-vectors from the connecting high-symmetry lines $\overline{\mathrm{M}}$-$\overline{\Gamma}$-$\overline{\mathrm{K}}$-$\overline{\mathrm{M}}$.

Along the line $\overline{\mathrm{M}}$-$\overline{\Gamma}$-$\overline{\mathrm{K}}$-$\overline{\mathrm{M}}$ we investigated the energetics within the Heisenberg model up the second nearest-neighbor interaction, i.e. including the exchange constants J_1, J_2. The results are summarized in Fig. 18 in terms of a zero-temperature phase diagram. Depending on the signs and values of J_1, and J_2 four kinds of possible magnetic ground states exist: FM, RW-AFM, $120°$, and the SSDW. If J_2 is zero or positive (ferromagnetic) than there are only two possible magnetic ground states, determined by the sign of J_1, the FM and the Néel state. But small values of J_2 are already sufficient to change the magnetic ground state and an infinite number of magnetic states becomes possible, the RW-AFM state or the incommensurable SSDW at any possible wave-vector $\mathbf{q}_{\|}$ at the high-symmetry line $\overline{\Gamma}$-$\overline{\mathrm{M}}$. Extending the model by including also J_3, a magnetic state with a $\mathbf{q}_{\|}$ at any high-symmetry line can become ground state.

Since the J's are rapidly varying functions of the number of d electrons, *ab initio* calculations

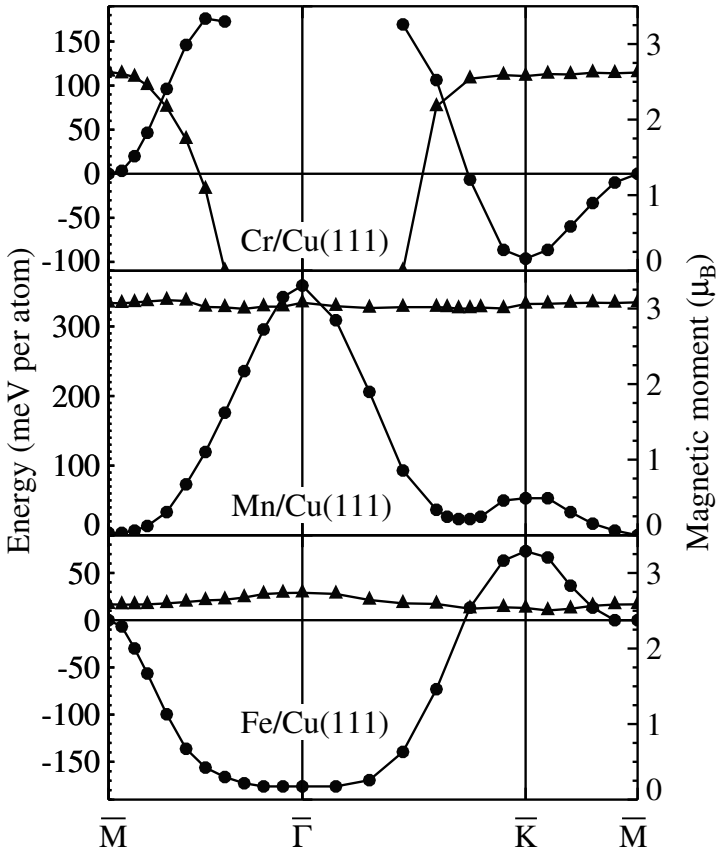

Fig. 23. *Calculated total energies (circles, left scale) and magnetic moments (triangles, right scale) for spin-spiral states in $3d$-UMLs with the Cu(111) geometry as function of the 2D wave vector $\mathbf{Q}_\parallel$ along the high symmetry lines of the 2DBZ. The energy is shown relative to the energy of the RW-AFM state.*

are carried out to determine the element specific ground states. Since the calculations are very time comsuming, the full overview has been worked out only for unsupported, free-standing monolayers (UML). Fig. 23 shows for the UMLs with the Cu lattice constant the total energy $E(\mathbf{Q}_\parallel)$ and the magnetic moments $M(\mathbf{Q}_\parallel)$ calculated for a discrete set of the spin-spiral $\mathbf{Q}_\parallel$ vectors along the high-symmetry lines. Among all the SSDWs calculated, the high-symmetry points have the lowest energies: the 120° Néel state ($\overline{\mathrm{K}}$-point) for Cr(111), the RW-AFM state ($\overline{\mathrm{M}}$-point) for Mn(111), and the FM state ($\overline{\Gamma}$-point) for Fe(111). For Fe and Mn, the $M(\mathbf{Q}_\parallel)$ are nearly a constant, but the Cr moments change drastically, as no ferromagnetic solution could be found for Cr(111). One more interesting observation is the local minimum of $E(\mathbf{Q}_\parallel)$ for Mn on the line $\overline{\Gamma}$-$\overline{\mathrm{K}}$, which is only 21 meV higher in energy than the RW-AFM state. We expect that a small change in the d-band filling, e.g. due to alloying with Fe, may change the energetics and an incommensurate SSDW may become the magnetic ground state.

For Mn, the lowest energy magnetic state found so far is the RW-AFM state, which corresponds to the commensurate SSDW state with one single $\mathbf{Q}_\parallel$-vector at the $\overline{\mathrm{M}}$-point of the 2DBZ, and the RW-AFM is also called single-$\mathbf{Q}_\parallel$ (1Q) state. In the 2DBZ there are three $\overline{\mathrm{M}}$-points corresponding to the three possible directions of the long axis of the RW-AFM unit cell on a triangular lattice. They are equivalent in symmetry, but are different to each other with $\mathbf{Q}_\parallel$-vectors, $\mathbf{Q}_\parallel^{(k)}$, for $k = 1, 2, 3$. Within the Heisenberg model the energy of each SSDW denoted by one of the three wave vectors $\mathbf{Q}_\parallel^{(k)}$ or any SSDW being an orthogonalized linear combination of those are degenerate. Higher order spin interactions (3) and (5) may lift this degeneracy and a so-called triple-$\mathbf{Q}_\parallel$ (3Q)-state, may become lower in energy. The 3Q-state is a three-dimensional non-collinear spin-structure on a 2D lattice (see Fig. 24) with four chemically identical atoms per surface unit-cell, where the relative angle between all nearest-neighbor spins is given by

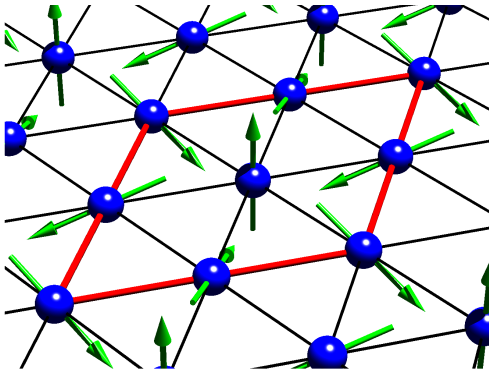

Fig. 24. *An image of the magnetic 3Q-structure, with spins pointing in all three directions of the spin-space. Note that, due to the neglect of the spin-orbit interaction only the relative orientation of the moments is specified.*

the tetrahedron angle of $109.47°$. The 3Q-state is formed as a linear combination of the three RW-AFM (1Q) structures orthogonal in spin-space, each having one of the three $\mathbf{Q}_{\parallel}^{(k)}$-vectors of the $\overline{\mathrm{M}}$-points:

$$\mathbf{m}(\mathbf{r}+\mathbf{R}_i) = m(\mathbf{r}) \times \frac{1}{\sqrt{3}} \sum_{k=1}^{3} e^{i\mathbf{Q}_{\parallel}^{(k)}\,\mathbf{R}_i}\,\hat{\mathbf{e}}^{(k)}, \tag{65}$$

where the $\hat{\mathbf{e}}^{(k)}$ are orthogonal unit vectors in spin space. We see that in the nearest-neigbhor approximation to the higher order exchange contributions the sign of K_1 and B_1 determine the sign of the energy difference $\Delta E = E_{3Q} - E_{1Q} = 16/3S^4(2K_1 + B_1)$ and thus whether the 3Q or the 1Q state becomes the magnetic ground state. From the *ab initio* calculations for the Mn UML in the geometry of Cu(111) we [53] found that the 3Q-state is 15 meV/atom lower in energy than the 1Q-state.
Calculations including the Cu(111) substrate show that the energy differences between different magnetic states change due to the present of the substrate, but the magnetic ground state remains unaltered: Cr/Cu(111) exhibits the 120° Néel state (2.35 μ_{B}), Mn/Cu(111) the 3Q-structure (2.74 μ_{B}), which is 17 meV lower in energy than the 1Q-state (3.00 μ_{B}), and Fe/Cu(111) is ferromagnetic (2.63 μ_{B}). On the Ag(111) substrate [114] the overall picture is the same, but two differences were noticed: V/Ag(111) is magnetic (2.19 μ_{B}) and exhibits as Cr/Ag(111) (3.65 μ_{B}) the 120° Néel state and the magnetic gound state of Mn/Ag(111) is the RW-AFM state (3.91 μ_{B}) and not the 3Q-state (3.88 μ_{B}). Fe/Ag(111) is ferromagnetic (3.02 μ_{B}). We believe that the complex spin-structures presented here, can be resolved using the spin-polarized scanning tunneling microscope in the constant-current mode [114, 115].

6.3 Chiral domain walls in Fe/W(110)

In this section, we illustrate the relevance of the DM interaction for the formation of chiral domain walls in Fe double layer (DL) on W(110), an ultrathin Fe film consisting of two atomic layers grown on the W(110)-surface. We choose this system, since its magnetic structure has been studied extensively by spin-polarized STM, cf. [116, 117, 118]. The magnetic pattern of the Fe DL on W(110) consists of a regular sequence of out-of-plane magnetized domains separated by domain walls [119, 45, 120]. The spatial orientation of the corresponding domain walls is determined by the crystal lattice and hardly influenced by the mesoscopic shape of the sample: The walls are preferably oriented normal to the $[001]$-direction (i.e. the magnetization changes along $[001]$ and remains constant along $[1\bar{1}0]$). In the following, we want to investigate this effect on the basis of the previously introduced micromagnetic model (50). If the DM term is irrelevant, the magnetization in the domain walls tries to avoid the hard axis and the

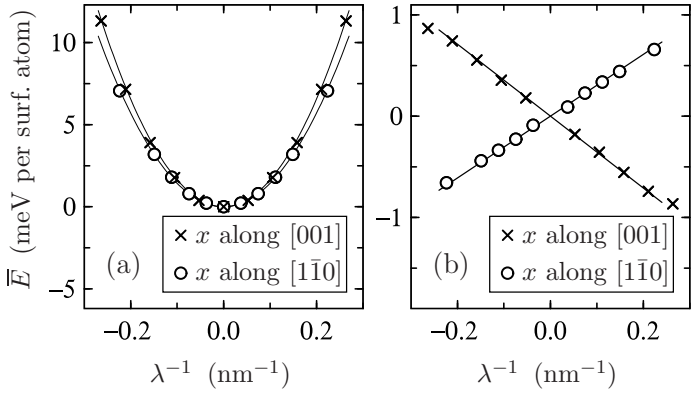

Fig. 25: *Energies of the homogeneous spin spirals obtained from electronic-structure calculations. The energies are plotted against the inverse of the period length λ. The results shown in (a) are obtained without spin-orbit interaction. Quadratic fits to these symmetric curves yield the spin stiffness A. (b) shows the odd part of $E(\lambda^{-1})$ obtained by including spin-orbit coupling. The slope of these curves at $\lambda^{-1} = 0$ correspond to D.*

magnetization rotation axis does not depend on the propagation direction. In this case, the energies $\sqrt{A\,K}$ of walls that are oriented in different crystallographic directions differ due to the spin stiffness, i.e. the value of A depends on the propagation direction. However, the values obtained for A by electronic-structure calculations do not change much for different propagations direction (cf. Fig. 25 left panel). A further indication of the relevance of the DM interaction in the studied system is the fact, that all domain walls that are observed within one sample show the same rotational direction [45, 120], this cannot be explained on the basis of symmetric exchange interactions. In the following we take the DM term into account, but we restrict our investigations to planar domain walls that can be described with the equations (50). If the propagation direction and the spin-rotation axis are both oriented along a high-symmetry line, we have to consider eight different walls that depend on six parameters. The walls are listed in Table 4 and their energies are given by equation $E = 4\sqrt{A\,K} - \pi\,|D|$.

We estimate values for the model parameters by electronic-structure calculations. A and D are obtained by using the approach introduced in Section 4.6. The results of these calculations are shown in Fig. 25. The anisotropy constant K consists of two main contributions, a term due to the anisotropic electronic energy and a term due to the magnetostatic interactions. The first term can be estimated directly from the electronic energies of collinear configurations with different spin quantization axes, the second term can be estimated from the summation of magnetic (dipole) moments Eq. (6). This sum converges fast, since we are considering a

	K_{001}		$K_{1\bar{1}0}$		
walls normal to [001] A_{001}	$+D_{001}$	$-D_{001}$	$D=0$	$D=0$	
walls normal to [1$\bar{1}$0] $A_{1\bar{1}0}$	$D=0$	$D=0$	$+D_{1\bar{1}0}$	$-D_{1\bar{1}0}$	[1$\bar{1}$0] [001]

Table 4: *Planar rotation path of domain-wall moments between two magnetic domains, with the magnetization pointing out-of-plane (⊗) or into-the plane (⊙), and corresponding model parameters.*

two-dimensional ultrathin magnetic film and not a magnetic bulk system. The results of our calculations are summarized in Table 5 (for further details cf. Ref. [46]). The values given for the spin-stiffness constants A are fairly accurate, since they are obtained from an unambiguous fitting procedure on a curve on a large energy scale (cf. Fig. 25). The values given for D are less accurate, but they tell us the order of magnitude of the Dzyaloshinskii vector. The accuracy of the anisotropy constants K is not satisfactory, these calculations reach the limit of our computational method and we cannot rule out an error of a few $\mathrm{meV\,nm^{-1}}$ (note that $1\ \mathrm{meV\,nm^{-2}} \mathrel{\widehat{=}} 0.035$ meV per Fe atom).

		001	$1\bar{1}0$
spin stiffness	$A\ /\ (\,\mathrm{meV}\,)$	58.8	51.1
DM interaction	$D\ /\ (\,\mathrm{meV\,nm^{-1}}\,)$	-8.0	6.9
anisotropy energy	$K\ /\ (\,\mathrm{meV\,nm^{-2}}\,)$	1.4	3.0

Table 5: *Theoretically predicted model parameters converted into areal densities. The crystallographic directions refer to the indices used in Table 4.*

Inserting the values given in Table 5 in equation $E = 4\sqrt{A\,K} - \pi\,|D|$ yields the wall energies

$$\begin{aligned} 4\sqrt{A_{001}\,K_{001}} - \pi\,|D_{001}| &= 11\ \mathrm{meV\,nm^{-1}}\ , \\ 4\sqrt{A_{001}\,K_{1\bar{1}0}} &= 53\ \mathrm{meV\,nm^{-1}}\ , \\ 4\sqrt{A_{1\bar{1}0}\,K_{001}} &= 34\ \mathrm{meV\,nm^{-1}}\ , \\ 4\sqrt{A_{1\bar{1}0}\,K_{1\bar{1}0}} - \pi\,|D_{1\bar{1}0}| &= 28\ \mathrm{meV\,nm^{-1}}\ . \end{aligned} \tag{66}$$

We find the observed wall orientation cannot be explained by the spin stiffness alone, and the DM interaction is strong enough to compete with the other quantities. According to the values given in Table 5 the lowest energy indeed corresponds to a wall oriented normal to the $[001]$ direction cf. Fig. 4 as observed experimentally. The negative sign of D_{001} corresponds to a right-rotating wall. The formation of a domain wall does not lower the energy of the system. This implies that the collinear state is the ground state. In agreement with SP-STM experiments we find walls with a specific rotational direction that are oriented normal to the $[001]$ direction. We identify these walls as right-rotating Néel-type walls. Based on the microscopic understanding we had been able to solve a longstanding open problem of why the domain orientation is sensitive to the underlying crystal structure rather than to the surface geometry. The studied system nicely illustrates the relevance of the Dzyaloshinskii-Moriya interactions for magnetic surfaces. Chiral domain walls are an important new type of domain-wall with interesting new properties relevant to concepts in information storage such as the racetrack memory concept.

Acknowledgements

I gladly acknowledge the discussions with Dr. Gustav Bihlmayer and Dr. Samir Lounis.

References

[1] M. Bode, M. Heide, K. von Bergmann, P. Ferriani, S. Heinze, G. Bihlmayer, A. Kubetzka, O. Pietzsch, S. Blügel, and R. Wiesendanger, Nature **447**, 190 (2007).

[2] J. Sticht, K. H. Höck, and J. Kübler, J. Phys.: Condens. Matter **1**, 8155 (1989).

[3] J. Kübler, *Theory of Itinerant Magnetism*, Oxford University Press (2000).

[4] L. M. Sandratskii and J. Kübler, Newsletter 14 (1996), http://www.psi-k.org/newsletters/-News_14/Highlight_14.pdf .

[5] L. M. Sandratskii, Adv. in Phys. **47**, 91 (1998).

[6] Ph. Kurz, F. Förster, G. Bihlmayer, S. Blügel, and L. Nordström, Newsletter **38** (2000), http://www.psi-k.org/newsletters/News_38/newsletter_38.pdf .

[7] Ph. Kurz, F. Förster, L. Nordström, G. Bihlmayer, and S. Blügel, Phys. Rev. B **69**, 024415 (2004).

[8] F. Schiller, D. V. Vyalikh, V. D. P. Servedio, and S. L. Molodtsov, Phys. Rev. B **70**, 174444 (2004).

[9] R. Hafner, D. Spisak, R. Lorenz and J. Hafner, Phys. Rev. B **65**, 184432 (2002).

[10] K. Hirai, J. Phys. Soc. Jpn. **62**, 690 (1993).

[11] E .O. Wollan and W. C. Koehler, Phys. Rev. **100**, 545 (1955).

[12] F. Keffer, Encyclopedia of Physics, Vol. 18/2, (1966) edited by H. P. J. Wijn (Berlin: Springer).

[13] J. M. D. Coey, Can. J. Phys. **65**, 1210, (1987).

[14] S. Geller, J. Chem. Phys. **24** 1236 (1956).

[15] T. Kimura, S. Ishihara, H. Shintani, T. Arima, K. T. Takahashi, K. Ishizaka, and Y. Tokura, Phys. Rev. B **68**, 060403 (2003).

[16] C. Zener, Phys. Rev. **82**, 403 (1951).

[17] C. Zener, Phys. Rev. **81**, 440 (1951).

[18] B. L. Gyorffy, A. J. Pindor, J. Staunton, G. M. Stocks and H. Winter, J. Phys. F **15**, 1337 (1985).

[19] V. P. Antropov, N. N. Harmon and A. N. Smirnov, J. Magn. Magn. Mater. **200**, 148 (1999).

[20] I. Dzyaloshinsky, J. Phys. Chem. Solids **4**, 241 (1958).

[21] T. Moriya, Phys. Rev. **120**, 91 (1960).

[22] A. N. Bogdanov, D. A.Yablonskii, Sov. Phys. JETP **68**, 101 (1989).

[23] A. Bogdanov and A. Hubert, J. Magn. Magn. Mater. **138**, 255 (1994).

[24] T.H.R. Skyrme, Nucl. Phys. **31**, 556 (1962).

[25] A. Hubert, R. Schäfer, *Magnetic Domains* (Springer-Verlag, Berlin, 1998).

[26] A. Fert, V. Cros and J. Sampaio, Nature Nanotech. **8**, 152 (2013).

[27] T. Schulz, R. Ritz, A. Bauer, M. Halder, M. Wagner, C. Franz, C. Pfleiderer, K. Everschor, M. Garst, A. Rosch, Nature Physics **8**, 301 (2012).

[28] Y. Aharonov and A. Stern, Phys. Rev. Lett. **69**, 3593 (1992).

[29] P. Bruno, Phys. Rev. Lett. **93**, 096806 (2004).

[30] S. Mühlbauer, B. Binz, F. Jonietz, C. Pfleiderer, A. Rosch, A. Neubauer, R. Georgii, P. Böni, Science **323**, 915 (2009).

[31] X. Z. Yu, Y. Onose, N. Kanazawa, J. H. Park, J. H. Han, Y. Matsui, N. Nagaosa, and Y. Tokura, Nature **465**, 901 (2010).

[32] C. Pappas, E. Lelièvre-Berna, P. Falus, P. M. Bentley, E. Moskvin, S. Grigoriev, P. Fouquet, B. Farago, Phys. Rev. Lett. **102**, 197202 (2009).

[33] N. Kanazawa, Y. Onose, T. Arima, D. Okuyama, K. Ohoyama, S. Wakimoto, K. Kakurai, S. Ishiwata, Y. Tokura, Phys. Rev. Lett. **106**, 156603 (2011).

[34] H. Wilhelm, M. Baenitz, M. Schmidt, U. K. Rößler, A. A. Leonov, A. N. Bogdanov, Phys. Rev. Lett. **107**, 127203 (2011).

[35] X. Z. Yu, N. Kanazawa, Y. Onose, K. Kimoto, W. Z. Zhang, S. Ishiwata, Y. Matsui, Y. Tokura, Nature Materials **10**, (2011).

[36] S. V. Grigoriev, N. M. Potapova, S.-A. Siegfried, V. A. Dyadkin, E.V. Moskvin, V. Dmitriev, D. Menzel, C. D. Dewhurst, D. Chernyshov, R. A. Sadykov, L. N. Fomicheva, A.V. Tsvyashchenko, Phys. Rev. Lett. **110**, 207201 (2013).

[37] K. Shibata, X. Z. Yu, T. Hara, D. Morikawa, N. Kanazawa, K. Kimoto, S. Ishiwata, Y. Matsui, Y. Tokura, Nature Nanotechnology **8**, 723 (2013).

[38] P. Bak and M. H. Jensen J. Phys. C: Solid State Phys. **13**, L881 (1980).

[39] P. Ferriani, K. von Bergmann, E.Y. Vedmedenko, S. Heinze, M. Bode, M. Heide, G. Bihlmayer, S. Blügel and R. Wiesendanger, Phys. Rev. Lett. **101**, 027201 (2008).

[40] K. von Bergmann, S. Heinze, M. Bode, E. Y. Vedmedenko, G. Bihlmayer, S. Blügel, R. Wiesendanger, Phys. Rev. Lett. **96**, 167203 (2006).

[41] K. von Bergmann, S. Heinze, M. Bode, G. Bihlmayer, S. Blügel, R. Wiesendanger, New J. Phys. **9**, 396 (2007).

[42] S. Heinze, K. von Bergmann, M. Menzel, J. Brede, A. Kubetzka, R. Wiesendanger, G. Bihlmayer, S. Blügel, Nature Physics **7**, 713 (2011).

[43] N. Romming, M. Menzel, C. Hanneken, J. E. Bickel, B. Wolter, K. von Bergmann, André Kubetzka, R. Wiesendanger, Science **341**, 636 (2013).

[44] Matthias Menzel, Yuriy Mokrousov, Robert Wieser, Jessica E. Bickel, Elena Vedmedenko, Stefan Blügel, Stefan Heinze, Kirsten von Bergmann, André Kubetzka, and Roland Wiesendanger Phys. Rev. Lett. **108**, 197204 (2012).

[45] A. Kubetzka, M. Bode, O. Pietzsch, and R. Wiesendanger, Phys. Rev. Lett. **88**, 057201 (2002).

[46] M. Heide, G. Bihlmayer, and S. Blügel, Phys. Rev. B **78**, 140403(R) (2008).

[47] G. Chen, J. Zhu, A. Quesada, J. Li, A. T. NDiaye, Y. Huo, T. P. Ma, Y. Chen, H.Y. Kwon, C. Won, Z. Q. Qiu, A. K. Schmid, and Y. Z. Wu Phys. Rev. Lett. **110**, 177204 (2013).

[48] Kh. Zakeri, Y. Zhang, J. Prokop, T.-H. Chuang, N. Sakr, W. X. Tang, and J. Kirschner Phys. Rev. Lett. **104**, 137203 (2010).

[49] W. Heisenberg, Z. Phys. **49**, 619 (1928).

[50] M. Takahashi, J. Phys. C **10**, 1289 (1977).

[51] J.J. Sakurai, Modern Quantum Mechanics Revised Edition (Addison-Wesley, Reading, MA, 1994).

[52] K. Yoshida and S. Inagaki, J. Phys. Soc. Japan **50**, 3268 (1981).

[53] Ph. Kurz, G. Bihlmayer, K. Hirai and S. Blügel, Phys. Rev. Lett. **86** , 1106 (2001).

[54] S.-W. Cheong and M. Mostovoy, Nature Materials **6**, 13 (2007).

[55] D. A. Smith, J. Magn. Magn. Mater. **1**, 214 (1976).

[56] A. Fert and P. M. Levy, Phys. Rev. Lett. **44**, 1538 (1980).

[57] A. Fert, Mater. Sci. Forum, **5960**, 439 (1990).

[58] M. Kataoka, O. Nakanishi, A. Yanase, and J. Kanamori, J. Phys. Soc. Jap. **53**, 3624 (1984).

[59] J. Bouaziz, M. dos Santos Dias, A. Ziane, M. Benakki, S. Blügel, S. Lounis, to be published (2014).

[60] P. Hohenberg and W. Kohn, Phys. Rev. **136**, B864 (1964).

[61] W. Kohn and L. J. Sham, Phys. Rev. **140**, A1133 (1965).

[62] U. von Barth and L. Hedin, J. Phys. C: Solid State Phys. **5**, 1629 (1972).

[63] S. Di Napoli, A. M. Llois, G. Bihlmayer, S. Blügel, M. Alouani, and H. Dreysse, Phys. Rev. B **70** 174418 (2004).

[64] I. Turek, J. Kudrnovský, M. Diviš, P. Franek, G. Bihlmayer, and S. Blügel, Phys. Rev. B **68**, 224431 (2003).

[65] D. J. Singh and J. Ashkenazi, Phys. Rev. B **46**, 11570 (1992).

[66] V. L. Moruzzi, J. F. Janak, and A. R. Williams, *Calculated Electronic Properties of Metals*, (Pergamon, New York, 1978).

[67] S. Shallcross, A. E. Kissavos, V. Meded, and A. V. Ruban, Phys. Rev. B **72**, 104437 (2005).

[68] Ph. Kurz, G. Bihlmayer, and S. Blügel, J. Phys.: Condens. Matter **14**, 6353 (2002).

[69] H. W. White, B. J. Beaudry, P. Burgardt, S. Legvold, and B. N. Harmon, AIP Conf. Proc. **29**, 329 (1975).

[70] G. Vignale and M. Rasolt, Phys. Rev. B **37**, 10685 (1988).

[71] H. A. Bethe and E. E. Salpeter, *Quantum Mechanics of One- and Two-Electron Systems* (New York, Plenum 1977).

[72] T. Thonhauser, D. Ceresoli, D. Vanderbilt, and R. Resta, Phys. Rev. Lett. **95**, 137205 (2005).

[73] I. Yang, S. Y. Savrasov, and G. Kotliar, Phys. Rev. Lett. **87**, 216405 (2001).

[74] J. Stöhr, J. Magn. Magn. Mater. **200**, 470 (1999).

[75] G. Bihlmayer in: *Magnetism goes Nano, Schriften des FZ-Jülich: Matter and Materials (26)* (Jülich, 2005).

[76] M. Weinert, R. E. Watson, and J. W. Davenport, Phys. Rev. B **32**, 2115 (1985).

[77] V. P. Antropov, M. I. Katsnelson, M. van Schilfgaarde, and B. N. Harmon, Phys. Rev. Lett. **75**, 729 (1995).

[78] V. P. Antropov, M. I. Katsnelson, B. N. Harmon, M. van Schilfgaarde, and D. Kusnezov, Phys. Rev. B **54**, 1019 (1996).

[79] G. M. Stocks, B. Újfalussy, X.-D. Wang, Y. Wang, D. M. C. Nicholson, W. A. Shelton, A. Canning, and B. L. Györffy, Phil. Mag. B **78**, 665 (1998).

[80] P. H. Dederichs, S. Blügel, R. Zeller, and H. Akai, Phys. Rev. Lett. **53**, 2512 (1984).

[81] B. Újfalussy, X.-D. Wang, D. M. C. Nicholson, W. A. Shelton, G. M. Stocks, Y. Wang, and B. L. Györffy, J. Appl. Phys. **85**, 4824 (1999).

[82] P. W. Anderson, *Theory of Magnetic Exchange Interactions: Exchange in Insulators and Semiconductors*, Solid State Physics **14**, 99 (1963).

[83] K. Yosida, *Theory of Magnetism* (Spinger, Berlin-Heidelberg, 1996).

[84] C. Herring, in *Magnetism*, (Ed. G. Rado and H. Suhl) (Academic, New York, 1966).

[85] L. M. Sandratskii, Phys. Status Solidi B **136**, 167 (1986).

[86] L. M. Sandratskii, J. Phys.: Condens. Matter **3**, 8565 (1991).

[87] N. Ashcroft and N. Mermin, *Solid State Physics* (Saunders College, Philadelphia, 1976).

[88] M. Ležaić, P. Mavropoulos, G. Bihlmayer, and S. Blügel, Phys. Rev. B **88**, 134403 (2013).

[89] A. I. Liechtenstein, M. I. Katsnelson, V. P. Antropov, and V. A. Gubanov, J. Magn. Magn. Mater. **67**, 65 (1987).

[90] A. R. Mackintosh and O. K. Andersen, *Electrons at the Fermi Surface*, page 149, ed. M. Springford, Cambridge Univ. Press, London (1980).

[91] M. Heide, G. Bihlmayer, and S. Blügel, Physica B **404**, 2678 (2009).

[92] N. M. Rosengaard and Börje Johansson, Phys. Rev. B **55**, 14975 (1997).

[93] M. Pajda, J. Kudrnovský, I. Turek, V. Drchal, and P. Bruno, Phys. Rev. B **64**, 174402 (2001).

[94] N. Metropolis, A. W. Rosenbluth, M. N. Rosenbluth, A. H. Teller, and E. Teller, J. Chem. Phys. **21**, 1087 (1953).

[95] I. Turek, J. Kudrnovský, G. Bihlmayer, and S. Blügel, J. Phys.: Condens. Matter **15**, 2771 (2003).

[96] E. Şaşıoğlu, L. M. Sandratskii, and P. Bruno, J. Appl. Phys. **98**, 063523 (2005).

[97] K. Sato, P. H. Dederichs, and H. Katayama-Yoshida, J. Supercond. **18**, 33 (2005).

[98] S. Lounis, Ph. Mavropoulos, P. H. Dederichs and S. Blügel, Phys. Rev. B **72**, 224437 (2005).

[99] S. Lounis, Ph. Mavropoulos, R. Zeller, P. H. Dederichs and S. Blügel, Phys. Rev. B **75**, 174436 (2007).

[100] S. Lounis, M. Reif, Ph. Mavropoulos, L. Glaser, P. H. Dederichs, M. Martins, S. Blügel and W. Wurth, Eur. Phys. Lett. **81**, 47004 (2008).

[101] S. Lounis, P. H. Dederichs and S. Blügel, Phys. Rev. Lett. **101**, 107204 (2008).

[102] T. Flores, M. Hansen, and M. Wuttig, Surf. Sci. **279**, 251 (1992).

[103] D. Tian, H. Li, S. Wu, F. Jona, and P. Marcus, Phys. Rev. B **45**, 3749 (1992).

[104] S. Andrieu, H. Fischer, M. Piecuch, A. Traverse, and J. Mimault, Phys. Rev. B **54**, 2822 (1996).

[105] D. Tian, A. Begley, and F. Jona, Surf. Sci. Lett. **273**, 393 (1992).

[106] I. Grigorov and J. Walker, J. Appl. Phys. **81**, 3907 (1997).

[107] I. Grigorov, J. Walker, M. Hawley, G. B. and M. Lutt, and M. Fitzsimmons, J. Appl. Phys. **83**, 7010 (1998).

[108] I. Grigorov, I.-L. Siu, M. Fitzsimmons, and J. Walker, Phys. Rev. Lett. **82**, 5309 (1999).

[109] A. Arrott, B. Heinrich, S. Purcell, J. Cochran, and L. Urquhart, J. Appl. Phys. **61**, 3721(1987).

[110] K. Ounadjela, P. Vennegues, Y. Henry, A. Michel, V. Pierron-Bohnes, and J. Arabski, Phys. Rev. B **49**, 8561 (1994).

[111] L. Zhang, M. Kuhn, and U. Diebold, Surf. Sci. **371**, 223 (1997).

[112] M. Albrecht, J. Pohl, H. Wider, E. Malang, J. Kohler, K. Friemelt, and E. Bucher, Surf. Sci. **397**, 354 (1998).

[113] M. Sambi and G. Granozzi, Surf. Sci. **426**, 235 (1999).

[114] S. Heinze, Ph. Kurz, D. Wortmann, G. Bihlmayer, and S. Blügel, Appl. Phys. A **75**, 25 (2002).

[115] D. Wortmann, S. Heinze, Ph. Kurz, G. Bihlmayer, and S. Blügel, Phys. Rev. Lett **86**, 4132 (2001).

[116] M. Pratzer, H. J. Elmers, M. Bode, O. Pietzsch, A. Kubetzka, and R. Wiesendanger, Phys. Rev. Lett. **87**, 127201 (2001).

[117] M. Bode, Rep. Prog. Phys. **66**, 523 (2003).

[118] E. Y. Vedmedenko, A. Kubetzka, K. von Bergmann, O. Pietzsch, M. Bode, J. Kirschner, H. P. Oepen, and R. Wiesendanger, Phys. Rev. Lett. **92**, 77207 (2004).

[119] M. Bode, O. Pietzsch, A. Kubetzka, S. Heinze, and R. Wiesendanger, Phys. Rev. Lett. **86**, 2142 (2001).

[120] A. Kubetzka, O. Pietzsch, M. Bode, and R. Wiesendanger, Phys. Rev. B **67**, 020401(R) (2003).